Postprint of: Śmiechowski M., Unusual Influence of Fluorinated Anions on the Stretching Vibrations of Liquid Water, JOURNAL OF PHYSICAL CHEMISTRY B, Vol. 122, Iss. 12 (2018), pp. 3141–3152

Unusual Influence of the Fluorinated Anions on the Stretching Vibrations of Liquid Water

Maciej Śmiechowski*

Department of Physical Chemistry, Chemical Faculty, Gdańsk University of Technology, Narutowicza 11/12, 80-233 Gdańsk, Poland

E-mail: Maciej.Smiechowski@pg.edu.pl

Abstract

Infrared (IR) spectroscopy is a commonly used and invaluable tool in the studies of solvation phenomena in aqueous solutions. Concurrently, ab initio molecular dynamics (AIMD) simulations deliver the solvation shell picture at a molecular detail level and allow for a consistent decomposition of the theoretical IR spectrum into underlying spatial correlations. Here, we demonstrate how the novel spectral decomposition techniques can extract important information from the computed IR spectra of aqueous solutions of BF_4^- and PF_6^-, interesting weakly-coordinating anions that have been known for a long time to alter the IR spectrum of water in an unusual manner. The distance-dependent spectra of both ions are analyzed using the spectral similarity method that provides a quantitative picture of both the spectrum of the solute-affected solvent and the number of solvent molecules thus altered. We find, in accordance with previous experiments, a considerable blue shift of the ν_{OH} stretching band of liquid water by 264 cm^{-1} for BF_4^- and 306 cm^{-1} for PF_6^-, with the affected numbers being 3.7 and 4.2, respectively. Considering also the supplementary information on solute–solvent dipolar couplings delivered by radially- and spatially-resolved IR spectra, the computational IR spectroscopy based on AIMD simulations is shown to be a viable predictive tool with strong interpretative power.

Introduction

Aqueous ionic solutions have always attracted considerable attention in physical chemistry, as the water's ability to solvate ionic species is of great relevance to the chemistry of life.[1–3] Since the 1950s the discussion of the influence of ions on water has often been associated with the idea of the predominantly structural effect exerted by ions on the solvent, resulting in the popularity of the terms structure making and breaking.[4,5] Unfortunately, this simplistic concept has continued to lead to vague definitions, primarily because different experimental methods seem to provide somewhat differing concepts of what really means a

structure maker/breaker. On the basis of the most current diffraction data, the entire idea of structure making and breaking seems to need a redefinition.[6] Particularly the emergence of ultrafast time-resolved vibrational spectroscopic techniques, allowing direct access to the time scales on which the structural dynamics of aqueous solutions takes place, opened up a new dimension in the studies of aqueous electrolytes.[7]

The possible water structure breaking is often mentioned for BF_4^- and PF_6^-, the anions being the subject of this study. Nowadays, they find industrial applications in two important areas, namely as anions in lithium salts for Li-ion batteries[8] and as counterions of the bulky organic cations in room temperature ionic liquids.[9] Their peculiar properties in aqueous solution were noticed quite early in vibrational spectroscopic experiments.[10–15] Namely, both anions were found to extremely blue-shift the stretching band of water (viz., 2644 cm^{-1} for BF_4^-[10] and 2667 cm^{-1} for PF_6^-[11] vs. 2509 cm^{-1} for bulk water[16] for the ν_{OD} band of HDO isotopically diluted in H_2O; note that all band shifts in this work are referenced to the bulk liquid water stretching band position). Since the predicted ν_{OD} band position for HDO molecule in H_2O not forming any hydrogen bonds (H-bonds) is 2644 cm^{-1},[16] it was previously argued that the anion–water interactions for BF_4^- and PF_6^- are dominated by dispersion and any H-bonding must be extremely weak.[10,11] Additionally, the dynamics of anion–water H-bond exchange was measured for both anions with two-dimensional (2D) infrared (IR) spectroscopy.[17–20] The orientational relaxation time for water H-bonded to the anion is 5 ps for BF_4^- and 7.6 ps for PF_6^-, in comparison to 2.6 ps for bulk water.[17,19,20] Somewhat surprisingly, even though the static IR spectroscopy indicates very weak H-bonding, the time-resolved studies clearly demonstrate that water reorientation dynamics is retarded by both anions.

This seemingly counterintuitive conclusions have been recently resolved in our force field MD study of aqueous $NaBF_4$ and $NaPF_6$.[21] Both the weakening of the hydrogen bond network of water around the solutes postulated previously from the static IR spectra[10,11] and the severely retarded rotational relaxation of the solvent in the hydration shells measured in

pump–probe experiments[17,19] have been shown to be equally true and essentially independent phenomena. However, in order to look in more detail into the modulation of the IR spectrum of the solvent by the studied solutes we turn here to ab initio molecular dynamics (AIMD) simulations,[22] which were found previously to provide an excellent description of simple aqueous ions.[23–25] In this work, the previously developed formalism of distance-dependent and radially resolved spectra for a solute–solvent system[24–28] is applied to aqueous BF_4^- and PF_6^- in order to further confirm their unique influence on the water's IR spectrum.

Spatially-Resolved IR Spectra Analysis

The idea that solute–solvent interactions lead to specific changes in the computational IR spectra that can be identified when decomposing the total spectrum of the entire system is well attested and has helped to obtain the relevant contributions to the IR spectrum.[29,30] Recently, a rigorous derivation for solute–solvent systems has been published that allows for a systematic decomposition of the effect of the solute on the surrounding solvent in terms of distance-dependent or radially-resolved IR spectra.[24,25] It is based on the methodology originally employed for describing IR absorption modulation in bulk liquid water.[27,28] Here, we briefly review for the sake of completeness the original spectra decomposition procedure that leads to the distance-dependent IR spectra in the solute-centered frame and further supplement it with the fully three-dimensional picture utilizing the possibility to define a local molecular reference frame by the polyatomic BF_4^- and PF_6^- anions.

Spatially-resolved IR Spectra in a Solute–Solvent System

In linear response theory, the isotropic IR absorption coefficient is obtained as a Fourier transform of the time correlation function (TCF) of the (classical) total dipole moment, $\boldsymbol{M}(t)$. However, in a charged system the total dipole moment time derivative, $\dot{\boldsymbol{M}}(t)$, is preferred for various reasons discussed in detail in ref 24, so that the linear absorption

coefficient, $\alpha(\omega)$, is calculated as,

$$\alpha(\omega)\, n(\omega) = \mathcal{F}(\omega) \int_{-\infty}^{\infty} dt\, e^{-i\omega t} \left\langle \dot{\boldsymbol{M}}(t)\dot{\boldsymbol{M}}(0) \right\rangle \ , \tag{1}$$

where $n(\omega)$ is the refractive index of the sample, the angle brackets denote ensemble averaging and $\mathcal{F}(\omega)$ is a quantum correction prefactor to the classical TCF that makes it satisfy the 'detailed balance' condition.[31] Here, we apply the so-called harmonic approximation,

$$\mathcal{F}(\omega) = \frac{1}{4\pi\epsilon_0} \frac{2\pi}{3Vck_BT} \operatorname{sinc}^{-2}\left(\frac{\omega\delta t}{2}\right) \ , \tag{2}$$

for the system with the volume V and at the temperature T with other symbols denoting the usual fundamental constants. The last factor comes from the approximation of the genuine total dipole moment time derivative via finite differences, $\dot{\boldsymbol{M}}(t) \approx \delta\boldsymbol{M}(t)/\delta t$, where δt is the time step of the dipole moment trajectory. This is a direct consequence of MLWFs being discretely sampled along the system's trajectory with their exact velocities unknown (see ref 24 for details).

The total dipole moment of a system can be formally decomposed into effective molecular dipole moments, $\boldsymbol{M}(t) = \sum_{i=1}^{N} \boldsymbol{\mu}_i(t)$, calculated using the MLWFs centers. For a single ion in liquid water we may rewrite this decomposition as,

$$\dot{\boldsymbol{M}}(t) = \dot{\boldsymbol{\mu}}_{\mathrm{ion}}(t) + \dot{\boldsymbol{\mu}}_{\mathrm{wat}}(t) = \dot{\boldsymbol{\mu}}_{\mathrm{ion}}(t) + \sum_{i}^{\mathrm{water}} \dot{\boldsymbol{\mu}}_i(t) \ . \tag{3}$$

This approach allows for the simple decomposition of the total TCF into auto- and cross-correlations of the ion and water contributions,

$$\begin{aligned} C_{\mathrm{MM}}(t) = \left\langle \dot{\boldsymbol{M}}(t)\dot{\boldsymbol{M}}(0) \right\rangle = C_{\mathrm{ii}}(t) + C_{\mathrm{ww}}(t) + C_{\mathrm{iw}}(t) = \\ = \langle \dot{\boldsymbol{\mu}}_{\mathrm{ion}}(t)\dot{\boldsymbol{\mu}}_{\mathrm{ion}}(0) \rangle + \langle \dot{\boldsymbol{\mu}}_{\mathrm{wat}}(t)\dot{\boldsymbol{\mu}}_{\mathrm{wat}}(0) \rangle + 2 \langle \dot{\boldsymbol{\mu}}_{\mathrm{wat}}(t)\dot{\boldsymbol{\mu}}_{\mathrm{ion}}(0) \rangle \ , \end{aligned} \tag{4}$$

that are responsible for the respective contributions to the total IR spectrum that can be obtained by separate Fourier transforms of the three terms,

$$\alpha_{\mathrm{ion}}(\omega)\, n(\omega) = \mathcal{F}(\omega) \int_{-\infty}^{\infty} dt\, e^{-i\omega t}\, C_{\mathrm{ii}}(t) \tag{5}$$

$$\alpha_{\mathrm{wat}}(\omega)\, n(\omega) = \mathcal{F}(\omega) \int_{-\infty}^{\infty} dt\, e^{-i\omega t}\, C_{\mathrm{ww}}(t) \tag{6}$$

$$\alpha_{\mathrm{iw}}(\omega)\, n(\omega) = \mathcal{F}(\omega) \int_{-\infty}^{\infty} dt\, e^{-i\omega t}\, C_{\mathrm{iw}}(t)\ . \tag{7}$$

As a generalization of this approach, instead of a discrete partitioning according to eq 3 the total dipole moment derivative can be smoothly decomposed on a regular spatial grid $\boldsymbol{r}$ in the form of a continuous local dipole velocity density,[27,28]

$$\boldsymbol{\rho}(t, \boldsymbol{r}) = \sum_{i=1}^{N} \dot{\boldsymbol{\mu}}_i(t) \frac{1}{(2\pi\sigma^2)^{1.5}} \exp\left[-\frac{(\boldsymbol{R}_i(t) - \boldsymbol{r})^2}{2\sigma^2} \right]\ , \tag{8}$$

where $\boldsymbol{R}_i(t)$ is the center of mass (CoM) position of the ith molecule at time t, the σ parameter controls the width of the three-dimensional Gaussian projection of the density, and the decomposition is performed on a regular cubic grid $\boldsymbol{r}$. Note that the total dipole velocity is recovered by integration, $\dot{\boldsymbol{M}}(t) = \int_V d\boldsymbol{r}\, \boldsymbol{\rho}(t, \boldsymbol{r})$.

Here, as before,[24,25] we take advantage of the two-component nature of the studied systems and introduce an ion-centered TCF,

$$C_{\mu\rho}(t, \boldsymbol{r}) = \langle \boldsymbol{\rho}(t, \boldsymbol{r}) \dot{\boldsymbol{\mu}}_{\mathrm{ion}}(0, 0) \rangle\ , \tag{9}$$

thus choosing the single solute molecule placed at the origin of the coordinate system as a natural reference point. At variance to the previous approach, we demand the local reference frame to be consistently set by the central molecule geometry. This requires the possibility to define a local Cartesian coordinate system within the solute molecule and explains, why it was not used previously, when only spherically symmetric halide ions were

addressed. The discussed TCF captures the dipolar *cross*-correlations between the solute and the surrounding solvent from the point of view of a fixed, non-rotating solute molecule. Simultaneously, another possibility to visualize local dipolar correlations and a counterpart to the solvent–density TCF introduced in eq 9 is to apply the local density–density TCF defined as,

$$C_{\rho\rho}(t, \boldsymbol{r}) = \langle \boldsymbol{\rho}(t, \boldsymbol{r}) \boldsymbol{\rho}(0, \boldsymbol{r}) \rangle \ , \tag{10}$$

that in turn describes the local *auto*-correlations of the projected dipole velocity density. This allows for a detailed insight into the local IR excitations of the solvent as seen from the point of view of the solute.

Fourier transforming the TCFs defined above, we ultimately obtain two variants of the spatially-resolved IR spectrum of the system,

$$\alpha_{\times}(\omega, \boldsymbol{r})\, n(\omega) = \mathcal{F}(\omega) \int_{-\infty}^{\infty} dt\, e^{-i\omega t}\, C_{\mu\rho}(t, \boldsymbol{r}) \tag{11}$$

$$\alpha_{\rho}(\omega, \boldsymbol{r})\, n(\omega) = \mathcal{F}(\omega) \int_{-\infty}^{\infty} dt\, e^{-i\omega t}\, C_{\rho\rho}(t, \boldsymbol{r}) \tag{12}$$

The absorption coefficients thus defined enable either a detailed analysis of the local contributions of the solvation shells to the "cross" IR spectrum due to correlated or *anti*-correlated solute–solvent dipolar oscillations that give rise to positive or negative contributions to the total IR spectrum (eq 11) or the unprecedentedly accurate picture of local solvent excitations around the solute molecule as captured by the fluctuating dipole velocity density (eq 12). Note, however, that neither approach leads to the total IR spectrum upon volume integration. Instead, integrating eq 11 one obtains a *cross*-correlation spectrum between the solute and the total dipole moment derivative of the system,

$$\begin{aligned} \alpha_{\times}(\omega)\, n(\omega) = \int \mathrm{d}^3\boldsymbol{r}\, \alpha_{\times}(\omega, \boldsymbol{r})\, n(\omega) = \mathcal{F}(\omega) \int_{-\infty}^{\infty} dt\, e^{-i\omega t} \langle \dot{\boldsymbol{M}}(t) \dot{\boldsymbol{\mu}}_{\mathrm{ion}}(0) \rangle = \\ = \alpha_{\mathrm{ion}}(\omega)\, n(\omega) + \alpha_{\mathrm{iw}}(\omega)\, n(\omega) \ . \end{aligned} \tag{13}$$

On the other hand, integration of eq 12 does not lead to the total IR spectrum or any well-defined subset of it, since it neglects cross-correlations between different points in Cartesian space. Nevertheless, the two variants of the spatially-resolved IR spectrum carry meaningful information about the solute–solvent interactions that can be detected experimentally, as discussed later.

For completeness, we also note in passing that for isotropic and spatially homogeneous systems the angular part of the solvent–density TCF from eq 9 might be integrated out to leave only the radial dependence on the distance from the solute, viz.

$$C^{\mathrm{rad}}_{\mu\rho}(t,r) = \langle \boldsymbol{\rho}(t,r,\Omega)\dot{\boldsymbol{\mu}}_{\mathrm{ion}}(0,0)\rangle = 4\pi r^2 \langle \boldsymbol{\rho}(t,r)\dot{\boldsymbol{\mu}}_{\mathrm{ion}}(0,0)\rangle \ , \tag{14}$$

thus giving rise to the radially-resolved "cross" IR spectrum,

$$\alpha_{\times}(\omega,r)\, n(\omega) = \mathcal{F}(\omega) \int_{-\infty}^{\infty} dt\, e^{-i\omega t}\, C^{\mathrm{rad}}_{\mu\rho}(t,r) \ , \tag{15}$$

that was used previously the disentangle the solvation shell contributions to the IR spectra of halide anions in aqueous solutions.[24,25]

Distance-dependent IR spectra

Another of the proposed decomposition schemes for solute–solvent systems takes advantage of the possibility to smoothly extract a finite spherical region around an ion and calculate the dipole moment within,

$$\dot{\boldsymbol{\mu}}^{\mathrm{R}}_{\mathrm{ion}}(t) = \mathcal{N}^{\mathrm{R}}_{\mathrm{ion}}(t) \left(\dot{\boldsymbol{\mu}}_{\mathrm{ion}}(t) + \sum_{i}^{\mathrm{water}} P_{\mathrm{ion},i}(t)\dot{\boldsymbol{\mu}}_i(t) \right) \ , \tag{16}$$

where the solvent molecules are selected using Fermi's cutoff function, $P_{\mathrm{ion},i}(t) = 1/\{1 + \exp[(R_{\mathrm{ion},i}(t) - R_c)/D]\}$, controlled by the cutoff radius R_c and the sharpness D. $R_{\mathrm{ion},i}(t)$ is the solute–solvent CoM distance for the water molecule i and the distance-dependent dipole

moment is normalized to a single absorbing molecule with the possibly fractional number of the neighboring solvent molecules, $\mathcal{N}^{\mathrm{R}}_{\mathrm{ion}}(t) = [1 + \sum_i P^2_{\mathrm{ion},i}(t)]^{-0.5}$, which is continuous in time. The fractional dipole moment of the system as defined in eq 16 gives ultimately rise to the distance-dependent absorption coefficient of the ion-containing region,

$$\alpha^{\mathrm{R}}_{\mathrm{ion}}(\omega, R_c)\, n(\omega) = \mathcal{F}(\omega) \int_{-\infty}^{\infty} dt\, e^{-i\omega t} \left\langle \dot{\boldsymbol{\mu}}^{\mathrm{R}}_{\mathrm{ion}}(t) \dot{\boldsymbol{\mu}}^{\mathrm{R}}_{\mathrm{ion}}(0) \right\rangle \ . \tag{17}$$

In the large cutoff limit ($R_c \to \infty$) the distance-dependent dipole moment has a limiting behavior $\dot{\boldsymbol{\mu}}^{\mathrm{R}}_{\mathrm{ion}}(t) \to \dot{\boldsymbol{M}}(t)/\sqrt{N}$, as easily seen from eq 16 taking $P_{\mathrm{ion},i}(t) \to 1$. Therefore, the total IR absorption spectrum from eq 1 is rigorously recovered from multiplication, $\alpha(\omega)\, n(\omega) = N\, \alpha^{\mathrm{R}}_{\mathrm{ion}}(\omega, R_c \to \infty)\, n(\omega)$. The most interesting, however, is the intermediate separation regime, where R_c is on the order of the solvation shell separation from the solvent. There, $\alpha^{\mathrm{R}}_{\mathrm{ion}}(\omega, R_c)$ probes the distinct response of the solvation shell water molecules together with the ion. In this way, the solvent most spectrally affected by the solute can be unambiguously characterized provided that the cutoff radius R_c is properly selected. Additionally, this offers a way to compare to the experimental IR data obtained from the difference spectra method that also numerically extracts solute-affected solvent spectrum by analyzing a series of solution spectra measured for increasing concentrations of the solute.[32,33] Recently,[26] we proposed to find the boundary value of the cutoff radius, R°_c, by application of the chemometric procedure based on Malinowski's spectral isolation algorithm[34] and known as the spectral similarity method (SSM).[35,36] Namely, a series of spectra with monotonically changing R_c values can be subjected to SSM in order to find the boundary cutoff radius that separates the subset of distance-dependent spectra that do not contain a significant contribution of the bulk water spectrum from the subset that does contain such contribution. This particular R°_c value corresponds to a given average value of the sum of Fermi cutoffs for the water molecules ($N^{\circ}_{\mathrm{ion}} = \sum_i P_{\mathrm{ion},i}(t)$, see above), so that it unambiguously provides the number of spectrally affected solvent molecules that can be directly compared with the experimentally

determined affected number.[32,33]

Finally, let us note that the refractive index dependence of the computed IR spectra can be easily removed with the help of the numerical Kramers–Krönig (KK) transform with only the knowledge of the optical frequency refractive index of the medium required.[24] Since $n(\omega)$ cannot be subject to the decomposition schemes presented above, any of the spatially-resolved or distance-dependent spectra may be corrected for dispersion effects only by dividing by the refractive index spectrum as obtained for the respective entire system.

Computational Methods

The studied systems consisted of 64 H_2O molecules and a single ion (Cl^-, BF_4^-, or PF_6^-) contained in a cubic cell with applied periodic boundary conditions. A pure water system (128 H_2O molecules) was simulated as a reference. Each system was initially prepared at the density of H_2O at 298 K (997 kg/m^3) and equilibrated for at least 3 ns in the isothermal-isobaric (NPT) ensemble using Tinker code (v. 6.3)[37] and employing the Amoeba force field definition of the water molecule and all ions.[38,39] The cell volume was then set to the average value from this run (discarding first 0.5 ns for equilibration, see Table 1) and further relaxed for 1 ns in the canonical (NVT) ensemble. Since the Amoeba force field provides good description of the studied fluorinated anions in liquid water,[21] we expect it to adequately relax the initial configuration.

AIMD simulations[22] were further carried out using the Quickstep electronic structure module[40] of the cp2k package (v. 2.3).[41,42] The electronic structure was described by density functional theory (DFT). The standard BLYP functional[43,44] was used together with an empirical dispersion correction in the DFT-D3 formalism.[45] The cutoff for the D3 correction was set to 20.0 Å. Quickstep implements a mixed Gaussian atomic orbitals/plane waves (GPW) representation of the electronic structure,[46] and we used a TZV2P basis set for atomic orbitals and a 600 Ry cutoff for the plane wave expansion of the electron density.

Explicit valence electrons were supplemented by norm-conserving GTH pseudo potentials.[47]

The systems were first equilibrated for 15 ps using a time step of 0.5 fs and at a slightly elevated temperature of 320 K in the NVT ensemble using massive Nosé-Hoover chain thermostatting.[22] This particular choice of the temperature for the employed functional/basis set combination was demonstrated previously to provide excellent agreement with the experimental data for bulk liquid water at 298 K.[48] After the equilibration period, 32 statistically independent initial conditions for each system (except pure H_2O, where 16 such configurations were used) were sampled every 2.5 ps from a further NVT simulation to initialize microcanonical (NVE) trajectories of 20 ps length each. During these runs the centers of maximally localized Wannier functions (MLWFs)[49] were computed in an on-the-fly manner[50] every 4 trajectory steps and molecular dipole moments were obtained on their basis. All analyzed observables have been averaged over the 32 independent NVE trajectories yielding canonical averages.

To obtain spatially-resolved IR spectra the local dipole densities according to eq 8 were computed on a cubic grid composed of 27^3 grid points (grid spacing ca. 0.485 Å) using $\sigma = 0.4$ Å. The distance-dependent dipole moment was calculated from eq 16 using $D = 0.25$ Å. All calculated spectra were smoothed for presentation by passing through a Gaussian filter with a standard deviation of 20 cm^{-1}. Numerical Kramers–Krönig transform was used to remove the refractive index contributions to the IR spectra,[24] using the experimental refractive index of H_2O, $n_D = 1.3325$.[51]

Results and Discussion

We begin the discussion with the results of the box volume relaxation during the initial force field MD simulations in the NPT ensemble, as summarized in Table 1. The partial molar volumes of the three anions in water were calculated directly from the converged box

volumes as

$$V_\Phi\,(\text{ion}) = V - 64V_\Phi^0\,(H_2O)\ , \tag{18}$$

where V is the average volume of the system and $V_\Phi^0\,(H_2O) = 18.06 \pm 0.02$ cm^3 mol^{-1} is the molar volume of pure AMOEBA water.[52] The $V_\Phi\,(\text{ion})$ values obtained in this work are compared with the experimental limiting apparent molar volumes in Table 1. The agreement

Table 1: Computed Partial Molar Volumes, Experimental Limiting Apparent Molar Volumes, and Converged Box Lengths for the Studied Aqueous Anions

Ion	V_Φ [a] (cm^3 mol^{-1})	V_Φ° (cm^3 mol^{-1})	L (Å)
Cl^-	24.9	23.2[b]	12.516
BF_4^-	44.6	50.6[c]	12.585
PF_6^-	64.8	60.8[c]	12.655

[a] Eq 18, estimated standard error 3.9 cm^3 mol^{-1}. [b] Ref 53. [c] Ref 54.

is generally within the estimated statistical error (apart from a marginally worse result for BF_4^-) and thus supports the applicability of the AMOEBA force field for the purpose of pre-equilibration of the studied systems.

The static structure of the hydration shells of the investigated anions is visualized with the help of radial distribution functions (RDFs), as seen in Figure 1(a) and 1(b) for anion–water oxygen and anion–water hydrogen pairs, respectively. For Cl^- we obtain the first

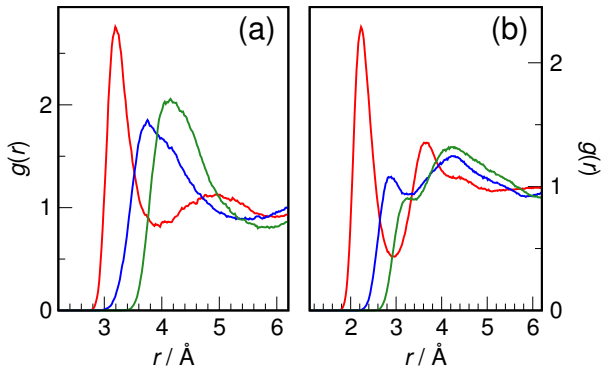

Figure 1: Radial distribution functions, $g(r)$, for (a) Cl$\cdots$O (red), B$\cdots$O (blue) and P$\cdots$O (green) pairs, as well as (b) Cl$\cdots$H (red), B$\cdots$H (blue) and P$\cdots$H (green) pairs.

maximum (corresponding to the most probable anion–water distance in the first hydration

shell) at $R_{\mathrm{ClO}} = 3.19$ Å and integration over the first peak in RDF gives the coordination number $N_{\mathrm{ClO}} = 7.0$. This anion is a perfect test case, since ample experimental data (chiefly from diffraction studies)[6,55–66] and previous AIMD investigations[24,67–80] are available for comparison. Experimentally, the Cl$\cdots$O distance is found in the range 3.1–3.2 Å, while the coordination number varies considerably from 5.6[55] to 7.4.[60] On the other hand, AIMD simulations predict a similar variation of both the Cl$\cdots$O distance (from 3.11 Å[68] to 3.22 Å[71]) and the corresponding coordination number (from 5.4[74] to 8.0[71]). The values reported here are consistently at the upper limit of both R_{ClO} and N_{ClO} found previously. However, dispersion-corrected functionals,[71] similarly to hybrid functionals,[70] are known to result in more expanded and less overstructured hydration shells of ions. Additionally, the accuracy of neutron diffraction measurements is most often estimated as at best ±0.1 Å for the interatomic distances and ±1.0 for coordination numbers.[6] Furthermore, measurements on the more dilute NaCl solutions deliver higher chloride coordination numbers, i.e., 7.0 to 7.3.[6,60] Concluding, the present results obtained for the static structure of the first hydration shell of Cl^- are in very good agreement with the experimental data.

In striking contrast to the well-studied chloride anion, no experimental measurements have been performed on the structure of the hydrated BF_4^- and PF_6^- anions. Thus, for comparison purposes we have to rely on the scarce force field MD studies available.[21,81] We obtain broad hydration shells for both anions, with the first maxima in the relevant RDFs located at $R_{\mathrm{BO}} = 3.75$ Å and $R_{\mathrm{PO}} = 4.15$ Å. These values lead to sizable coordination numbers obtained again by integration over the first peak, viz. $N_{\mathrm{BO}} = 18.9$ and $N_{\mathrm{PO}} = 23.0$. All these results are in excellent agreement with our recent study using the polarizable AMOEBA force field ($R_{\mathrm{BO}} = 3.71$ Å, $N_{\mathrm{BO}} = 17.6$, $R_{\mathrm{PO}} = 4.11$ Å, $N_{\mathrm{PO}} = 23.4$).[21] However, only a minor fraction of this coordinated water is actually H-bonded to the anion through its F atoms. Previously, we found that BF_4^- and PF_6^- form on average only 4.9 and 4.0 H-bonds with water, respectively.[21] In comparison, the much smaller Cl^- anion was found to form as many as 5.5 H-bonds with the first shell waters. Most importantly, the present

X$\cdots$H RDFs (see Figure 1) confirm the weakness of the first peaks for both BF_4^- and PF_6^-, further signifying the relatively low extent of anion–water H-bonding.[21]

The hydration structure of the studied anions might be in principle influenced by the limited system size available for AIMD simulations. However, we checked thoroughly (using the AMOEBA force field simulations) that the characteristic features of the discussed RDFs as shown in Figure 1 are well preserved for systems with varying number of water molecules, up to 512 H_2O. Further details of this comparison, including detailed figures, are available in the Supporting Information (SI).

While weak interaction with water may at first suggest insignificant influence of the solvent on the anions' electron density, in Figure 2(a) we show that this is clearly not the case. Both BF_4^- and PF_6^- are characterized with a significant induced dipole moment,

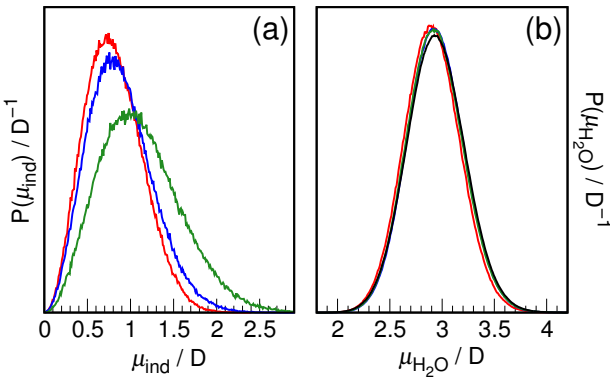

Figure 2: Normalized distribution functions of (a) the induced dipole moments of Cl^- (red), BF_4^- (blue) and PF_6^- (green) in aqueous solution calculated with respect to their center of mass and (b) the molecular dipole moments of water molecules in the first solvation shell of Cl^- (red), BF_4^- (blue) and PF_6^- (green) in comparison to bulk water (black).

greater than that of the chloride anion. For the latter, we find $\langle \mu_{\mathrm{ind}} \rangle = 0.81$ D by fitting to the Maxwell–Boltzmann distribution. This compares favorably with the previously reported values obtained from AIMD simulations (0.82 D[75] and 0.77 D,[24] the present distribution is also in an overall excellent agreement with the one shown in the latter work). Applying the same fit, we find $\langle \mu_{\mathrm{ind}} \rangle = 0.88$ D for BF_4^- and $\langle \mu_{\mathrm{ind}} \rangle = 1.11$ D for PF_6^-. These sizable induced dipole moments are comparable to those of the heavier halides (Br^- and I^-)[75,82]

and are decisive to the IR response of the solvated ions that captures the state of the water most perturbed by the presence of the solute, see below.

Previously, it was found that while water significantly polarizes anions (as discussed above), on the other hand ions barely polarize the surrounding water as far as its molecular dipole moment is considered to be the measure of this effect.[23–25,75,76,82] This observation is evident from Figure 2(b), where we show the distributions of the molecular dipole moments of first solvation shell waters. For the bulk liquid, we find $\langle \mu_{H_2O} \rangle = 2.94$ D by fitting to a normal distribution. This value is in excellent agreement with the previous AIMD investigations that predict average molecular dipole moment of liquid water in the range 2.9–3.1 D,[25,75,76,82–87] while the value ∼2.95 D seems to be reported most often.[75,76,84,86,87] Generally, the inclusion of exact exchange and/or dispersion corrections in the employed density functional is necessary to obtain accurate molecular dipole moments in liquid water simulations.[83] For Cl^-, we obtain $\langle \mu_{H_2O} \rangle = 2.90$ D for the water molecules in its hydration shell. The shift to lower values (by 0.04 D) is small, but consistent with earlier investigations, where similar shifts by −0.06 D to −0.12 D were found.[23,24,75,76] For the fluorinated anions in turn, the magnitude of the shift is barely significant, since we obtain $\langle \mu_{H_2O} \rangle = 2.93$ D and $\langle \mu_{H_2O} \rangle = 2.92$ D for water molecules in the BF_4^- and PF_6^- hydration shell, respectively. This indicates that the induced dipole moment of the ion and its ability to polarize water are apparently unrelated, as the already mentioned heavier halides (Br^- and I^-), although possessing similar dipole moments to the fluorinated anions studied here, clearly exert a stronger effect on the surrounding water than Cl^-.[23,75] Finally, we note that the width of the μ_{H_2O} distribution remains constant in all cases at ∼0.27 D (as measured by the standard deviation of the respective normal distributions) and this value is in excellent agreement with the previous studies.[75]

The molecular dipole moments are crucially important, since the dipolar correlations underlie the IR response (eq 1). It is instructive to look first at the IR spectra of the ions themselves. We have previously found that such spectra of polarizable solutes intimately

reflect the state of the solvent most perturbed by the solute (and the "solvent" here is not restricted to water).[24–26] In layman's terms, looking at the ion spectrum, one immediately sees the water spectrum. The IR spectra of the studied solutes calculated from eq 5 are shown in Figure 3 (in decadic molar absorptivity scale, i.e., $\varepsilon_{\mathrm{ion}}(\tilde{\nu}) = \alpha_{\mathrm{ion}}(\tilde{\nu})/\left(c_{\mathrm{ion}} \ln 10\right)$, where c_{ion} is the molar concentration in mol dm^{-3}). The AIMD spectrum of water has a maximum at

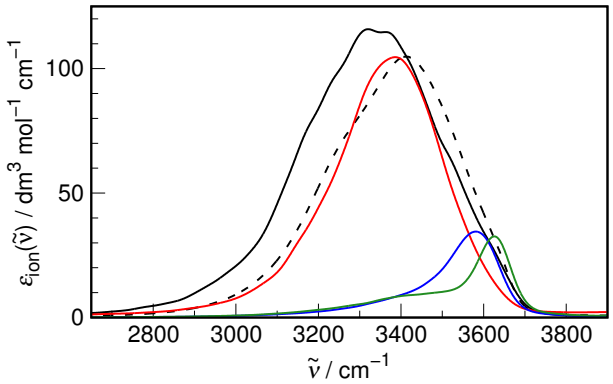

Figure 3: Infrared spectra of the solute, eq 5, in the water OH stretching vibrations range on the decadic molar absorptivity scale for Cl^- (red), BF_4^- (blue) and PF_6^- (green) compared with the bulk water spectrum (black), eq 1, and the experimental IR spectrum of water (black dashed, ref 88).

3320 cm^{-1}, to be compared with the experimental maximum found at 3413 cm^{-1}.[88] This magnitude of the red shift is typical of gradient-corrected functionals (even when dispersion effects are taken into account)[28,30,89,90] and explicit inclusion of nuclear quantum effects (which we neglect here) is required for better agreement with experiment.[91] On the other hand, all the studied ions cause a blue shift of the OH stretching band of water. While for Cl^- the band is moved by 66 cm^{-1} to higher wavenumbers and its maximum intensity is comparable to the bulk solvent, the spectra of the solvated fluorinated anions are drastically different. The blue shift amounts to 261 cm^{-1} for BF_4^- and 306 cm^{-1} for PF_6^- and both maximum and integrated intensity of the band is greatly suppressed. The state of the spectrally perturbed water as captured by the polarized solute is thus widely different from the bulk solvent.

Arguably, the system size limitations mentioned in the discussion of the RDFs are an

equally valid concern from the point of view of IR spectroscopy. While it is not easy to compare AIMD simulations with the force field ones when it comes to the intramolecular IR response of water, it is reasonable to expect that the vibrational dynamics itself, particularly in the far-IR spectral region, is fairly well represented even by typical simple force fields.[27] In the SI, we offer such a detailed comparison of the vibrational density of states of systems with an increasing number of water molecules, showing that it is practically unaffected by the system size. This in turn strongly suggests that the IR response of the hydrated anions, which is a result of both vibrational dynamics and dynamic polarization effects may be reasonably expected to be captured properly in the limited size systems tractable by AIMD simulations.

The experimental methods based on difference spectroscopy usually aim at obtaining the spectrum of the solute-affected solvent.[12,32,33] The relevant numerical bulk solvent spectrum subtraction procedure can be automatized and made assumption-free by applying chemometric analysis techniques, as demonstrated recently in our laboratory for the distance-dependent IR spectra obtained from AIMD simulations.[26] In Figures 4(a), 4(b), and 4(c) we present the sets of such spectra depending on the cutoff radius for Cl^-, BF_4^-, and PF_6^-, respectively. The boundary cutoff radii found chemometrically give rise to the characteristic distance-

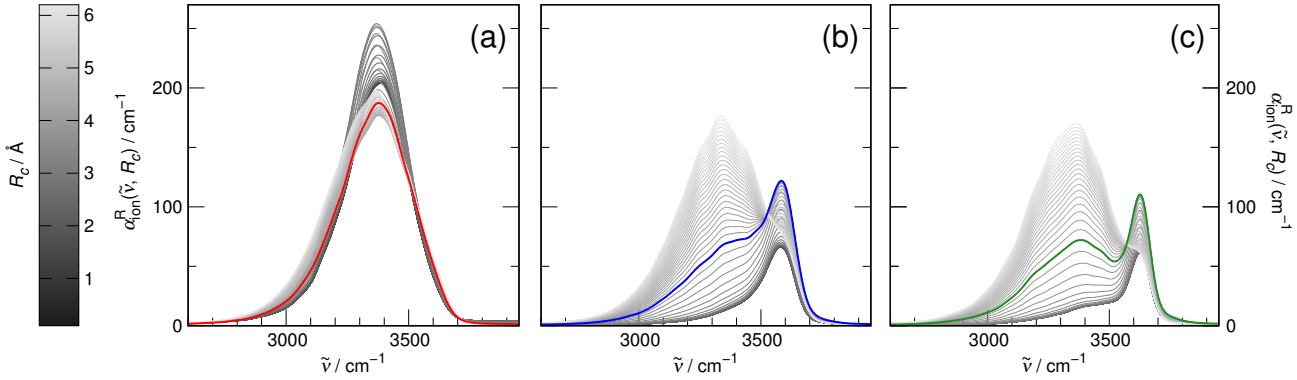

Figure 4: Distance-dependent IR spectra, eq 17, in the water OH stretching vibrations range for (a) Cl^-, (b) BF_4^- and (c) PF_6^-. The increasing cutoff radii (in the R_c = 0.1–6.2 Å range) are represented by the color gradient and the bold lines indicate the solute-affected spectra at the boundary cutoff radius value selected with the spectral similarity method for Cl^- (R_c° = 3.8 Å, red), BF_4^- (R_c° = 3.7 Å, blue) and PF_6^- (R_c° = 4.0 Å, green).

dependent spectra (indicated separately in the figure) that capture the state of the solvent perturbed by the solute while minimizing the contribution of the bulk solvent as a factor in the spectral decomposition.[26]

Focusing first on Cl^-, it is evident that the affected IR spectrum is not too different from the bulk water spectrum and is still very similar to the bare ion spectrum as shown in Figure 3. Indeed, the experimental data on aqueous chloride solutions confirm that the band position at maximum for Cl^--affected HDO in H_2O is blue-shifted by just $\sim$ 20 cm^{-1} (see ref 16 for a review of the data). From the distance-dependent spectra analysis we find the boundary cutoff radius of 3.8 Å, within which an average of 6.7 spectrally perturbed H_2O molecules can be found (see also Table 2 for a summary). The estimated uncertainty of R_c° is $\pm$0.3 Å, which provides an estimate of $\pm$1.0 for the N° value. While this may seem significant, note that it is comparable to the experimental uncertainty of the spectral isolation techniques,[32] as well as direct structure determination methods in the liquid phase.[4] A comparison with the $g_{\mathrm{ClO}}(r)$ RDF (see Figure 1) reveals that the N° value almost

Table 2: Comparison of the Experimental Shift of the HDO ν_{OD} Band Position at Maximum, $\Delta\tilde{\nu}^\circ_{\mathrm{exp}}$, with the Results of the Distance-dependent Spectra Analysis: Shift of the Water ν_{OH} Band Position at Maximum, $\Delta\tilde{\nu}^\circ_{\mathrm{MD}}$, Boundary Cutoff Radius, R_c°, and the Corresponding Sum of Fermi Cutoff Factors, N°, for the Studied Aqueous Anions

Ion	$\Delta\tilde{\nu}^\circ_{\mathrm{exp}}$ (cm^{-1})	$\Delta\tilde{\nu}^\circ_{\mathrm{MD}}$ (cm^{-1})	R_c° (Å)	N°
Cl^-	21[a]	58	3.8	6.7
BF_4^-	135[b]	264	3.7	3.7
PF_6^-	158[c]	306	4.0	4.2

[a] Ref 16. [b] Ref 10. [c] Ref 11.

exactly corresponds to the entire first hydration shell of aqueous chloride. Therefore, all the water molecules coordinated (H-bonded) to Cl^- contribute to the affected spectrum, as they sufficiently differ spectrally from the bulk solvent. Since for Cl^- the difference between the distance-dependent spectrum at R_c° and the bulk water spectrum is subtler than for BF_4^- and PF_6^-, in the SI we offer a supplementary figure showing the intensity modulation of the $\alpha^{\mathrm{R}}_{\mathrm{ion}}(\tilde{\nu}, R_c)$ spectra at 3320 cm^{-1} (the bulk water band position) with increasing R_c, as well

as a direct comparison of the $\alpha^{\mathrm{R}}_{\mathrm{ion}}(\tilde{\nu}, R_c^\circ)$ spectrum with the bulk water spectrum.

On the other hand, the particularly strong, albeit short-ranged influence of the fluorinated anions is apparent from Table 2. The extreme shifts of the maximum position of the water ν_{OH} band are in qualitative agreement with the previous experimental data concerning the ν_{OD} band shift of the isotopically diluted HDO in H_2O. The magnitude of the band shift for ν_{OH} is greater than for ν_{OD}, as expected basing on previous experimental and computational investigations.[92–94] In fact, the agreement is far more than qualitative, since the $\Delta\tilde{\nu}^\circ_{\mathrm{MD}}$ values are in perfect linear relationship with the $\Delta\tilde{\nu}^\circ_{\mathrm{exp}}$ ($R^2 \approx 1$), thus strongly suggesting that solely the isotopic effect is responsible for the difference in the two values in each case (see SI for the correlation plot and additional discussion). In contrast to Cl^-, the boundary cutoff radii correspond rather to the first maxima than to the subsequent minima of $g_{\mathrm{BO}}(r)$ and $g_{\mathrm{PO}}(r)$. Thus, owing to the very broad first hydration shells of both anions (cf. Figure 1), only a minor fraction of the coordinated water molecules are found to be spectrally affected. We also note that the present values of N° correspond perfectly with the experimental estimate of ca. 4 H_2O molecules affected by BF_4^-.[10] A similar value can be inferred indirectly for PF_6^- in aqueous HPF_6, for which the affected number of 10.4 has been found,[95] while the independent estimation gave $N = 6$ for the hydrated proton.[96]

Interestingly, the $\alpha^{\mathrm{R}}_{\mathrm{ion}}(\tilde{\nu}, R_c^\circ)$ spectra for BF_4^- and PF_6^- are composed of not only the extremely blue-shifted component, but contain also a significant contribution closer to the bulk H_2O band position. It is also blue-shifted with respect to the bulk and is in fact almost coincident with the Cl^--affected H_2O spectrum with $\Delta\tilde{\nu}^\circ_{\mathrm{MD}} \approx 60$ cm^{-1}. This milder blue shift can be ascribed to the second OH oscillator of an ion-affected water molecule (i.e., the one oriented towards the bulk of the solution). It is a consequence of the cooperative nature of the water H-bonds that leads to their weakening (or strengthening) in a concerted manner in the presence of H-bond acceptors of varying strengths; this phenomenon was also extensively tested experimentally.[97]

Apart from the characteristic distance-dependent spectrum that serves as a computa-

tional equivalent of the experimentally determined affected spectrum, it is also instructive to look at how the solute–solvent dipolar couplings shape the IR spectrum in the immediate vicinity of the solute. Let us first examine the radially-resolved IR spectra that already proved extremely insightful in the studies of ionic hydration.[24,25] The $\alpha_{\times}(\tilde{\nu}, r)$ spectra for Cl^-, BF_4^-, and PF_6^- are shown in Figures 5(a), 5(b), and 5(c), respectively. All of them

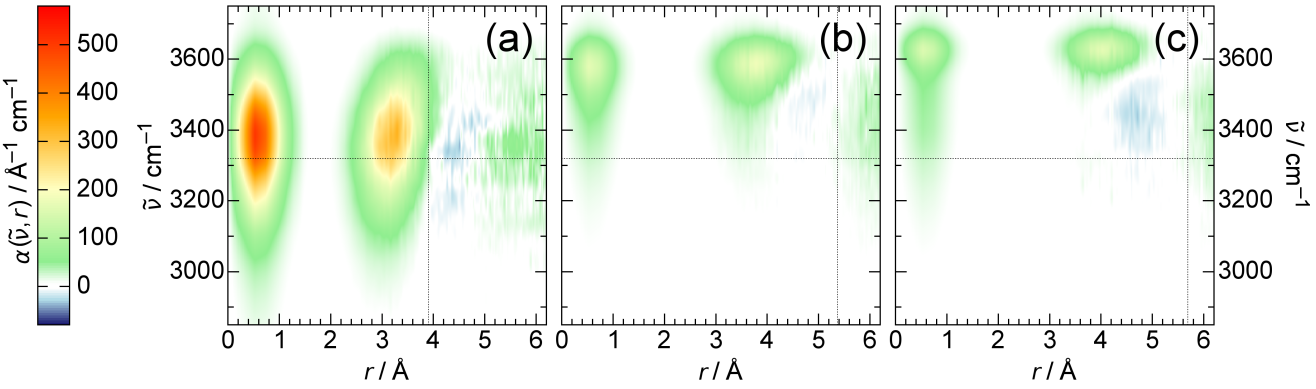

Figure 5: Radially-resolved IR spectra, eq 15, in the water OH stretching vibrations range for (a) Cl^-, (b) BF_4^- and (c) PF_6^-. Thin horizontal lines indicate the band position at maximum for bulk water, while thin vertical lines show the extent of the first hydration shells as inferred from the first minima in $g_{XO}(r)$ (see Figure 1).

are composed of a strong signal at low r that directly reflects the "self" term in the total IR spectrum, $\alpha_{ion}(\tilde{\nu})$ (eq 5, note that the expected response at $r = 0$ is effectively suppressed by the angular averaging via the $4\pi r^2$ term in eq 14). However, there is also a significant cross-correlation term between the solute and the surrounding solvent as indicated by the presence of a positive signal at r corresponding to the interior of the first hydration shell. It was found previously that the distance-dependent Kirkwood factor, $G_K(r)$, reaches a converged value in the 4–6 Å intermolecular separation range in the AIMD simulations of a bulk water system of the same size as studied here.[98] Thus, the dipolar correlations in this most crucial regime from the point of view of the present ion–water systems are expected to be representative of the situation in the bulk solution.

The differences found between Cl^- and the two fluorinated anions with respect to the boundary cutoff radii (see Table 2) can be seen clearly spotted also in the radially-resolved

IR spectra. For the chloride anion, the cross-correlation signal evidently encompasses the entire first hydration shell, spreading from ca. 2.5–4 Å (cf. Figure 1), while for BF_4^- and PF_6^- its intensity falls to zero well before the apparent hydration shell radius, so that only the few solvent molecules nearest to the anion are substantially coupled with its dipolar response. It is adequately explained by the fundamental differences between chloride and BF_4^- or PF_6^- with respect to the extent of the hydration shell and the number of H-bonds formed by water to the anion. While for chloride the first hydration shell is well-defined and there are only slightly less H-bonds to it than there are water molecules in the first shell,[21] for BF_4^- and PF_6^- the first hydration shells are quite extensive (cf. Figure 1), but the instantaneous number of H-bonds is much smaller, only 4–5.[21] The N° values obtained in this work are notably close to the latter values (cf. Table 2) and this strongly suggests that the appreciable influence on the surrounding water is restricted to the H-bonded H_2O molecules. It is clear from Figure 5, however, that in any case the large IR absorption of the studied polarizable solutes in aqueous solution in the water ν_{OH} vibrations range—where they are not expected to show any inherent activity due to the absence of the relevant intramolecular modes—is effectively induced by the molecules from the first hydration shell (or a subset of it). On the other hand, the ν_{OH} band position of these waters is heavily influenced by the solute, as found previously in numerous experiments,[16,99] although the polarization of the water by the solute is of minor importance (see Figure 2). These mutual solute–solvent spectral effects contribute heavily to the overall IR spectrum of the entire solution and their appreciation is thus crucial to our understanding of the way the IR response of the solutions is shaped by intermolecular interactions, as already noted before.[24,25]

Finally, let us note that in keeping with the well-established observations that ionic solutes exert a long range effect on the dipolar correlations in liquid water that goes beyond the simple structure making and breaking concept,[100] and that the cross-correlations in the solute–solvent dynamics must include the second hydration shell in order to fully explain the terahertz (THz) spectra of salt solutions,[23] we observe a distinct pattern of both anti-

and cross-correlations of molecular dipoles beyond the first hydration shell. These correlations, although of weak intensity, are already well-documented in the case of F^- and also Cl^-.[24,25] As seen in Figure 5, for the chloride anion this weaker modulation of the dipolar coupling falls entirely within the limits of the second hydration shell. However, the positive cross-correlation beyond $r = 5.5$ Å is located near the bulk water stretching band position, therefore its main effect on the shape of the distance-dependent spectra as seen in Figure 4(a) is just the intensity amplification of the main peak. A modified Figure 5(a) with a magnified IR intensity scale that better illustrates the correlations beyond the first hydration shell is available in the SI.

In contrast to Cl^-, the second hydration shell effects on either the distance-dependent or the radially resolved spectra of BF_4^- and PF_6^- cannot be expected to be captured by the systems of limited size studied in this work, since the maximum permissible cutoff radius of half the simulation cell length is just sufficient to encompass the entire first hydration shell, cf. Figure 1. On the other hand, the anti-correlation that is visible for Cl^- at the beginning of the second hydration shell in Figure 5 moves to the outer part of the first hydration shell for the fluorinated anions. The most plausible explanation is that this is a consequence of the general disruption of the H-bond network of water in the first hydration shell of these anions. This reflects the important structural differences between the first hydration shell of chloride and that of the fluorinated anions, discussed in detail above. Aqueous anions are in general seen to not only force the major shift of the water stretching band via strong solute–solvent coupling that results in positive feedback, but also shape the IR spectrum of the deeper layer of the solvent, although in a much more subtle way.

The well-defined molecular structures of BF_4^- and PF_6^- and their rigidity along the simulation trajectory allow us for the first time to test an extension to the insight offered by the radially-resolved spectra by examining the fully spatially-resolved spectra as defined in eqs 11 and 12. It is then possible to probe not just the distance dependence, but also the angular dependence of the solute–solvent dipolar couplings in the system. Addition-

ally, in contrast to the isotropic liquids that were studied in this respect previously,[27,101] the spatially-resolved spectra of aqueous solutes come in two slightly different, but supplementary varieties that enable the visualization of not only the solute–solvent response as an extension of the respective radially-resolved IR spectrum, but also the local autocorrelation of molecular dipole density on the grid, thus providing insight into the local IR excitations of the surrounding solvent. The relative drawback of such three-dimensional (3D) spectra is that it is no longer possible to include the entire spectral range in a single picture. However, by selectively probing the important frequencies in the IR range a very detailed description of the intermolecular couplings in the investigated frequency regimes can be obtained.[27,101]

The spatially-resolved IR cross- and autocorrelation spectra of aqueous fluorinated anions at the selected sampling frequency—corresponding to the maximum of the $\alpha_{\mathrm{ion}}(\tilde{\nu})$ spectrum (cf. Figure 3)—are shown in Figure 6 and 7, respectively. It is striking, how the positive

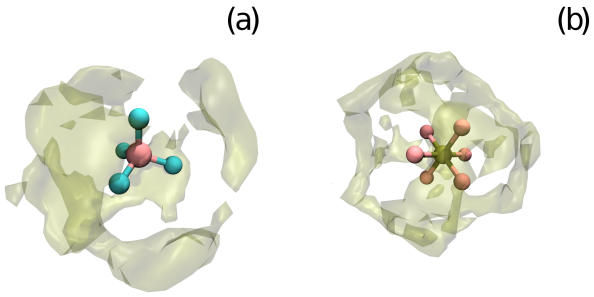

Figure 6: Spatially-resolved IR cross-correlation spectra, eq 11, for (a) BF_4^- at $\tilde{\nu} = 3580$ cm^{-1} and (b) PF_6^- at $\tilde{\nu} = 3625$ cm^{-1}, i.e., at the maxima of the respective IR spectra of the solute (see Figure 3). The reference frame is defined by the central molecule and the intramolecular contribution of the ion at the origin is removed for clarity. The isosurfaces are plotted at 30% of the maximum $\alpha_{\times}(\tilde{\nu}, \boldsymbol{r})$ intensity.

cross-correlation found within the first hydration shell of BF_4^- and PF_6^- in Figure 5 upon dropping the angular averaging reveals an intricate pattern of spatial domains, where the IR spectrum of the solute and the solvent is coupled due to a positive feedback (Figure 6(a) and 6(b) for BF_4^- and PF_6^-, respectively). Simultaneously, the 3D autocorrelation spectrum of the solvent itself shows nearly the same spatial arrangement (Figure 7(a) and 7(b) for BF_4^- and PF_6^-, respectively). It is apparent that the water molecules most efficiently vibrationally

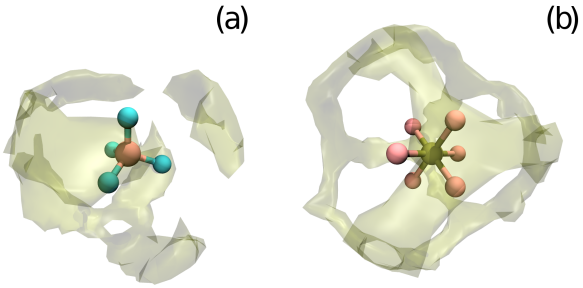

Figure 7: Spatially-resolved IR autocorrelation spectra, eq 12, for (a) BF_4^- at $\tilde{\nu} = 3580$ cm^{-1} and (b) PF_6^- at $\tilde{\nu} = 3625$ cm^{-1}, i.e., at the maxima of the respective IR spectra of the solute (see Figure 3). The reference frame is defined by the central molecule and the intramolecular contribution of the ion at the origin is removed for clarity. The isosurfaces are plotted at 60% of the maximum $\alpha_\rho(\tilde{\nu}, \boldsymbol{r})$ intensity.

coupled with the solute are preferentially located around the bisectors of FBF angles in BF_4^- or directly above the centers of the octahedron faces in PF_6^-. In either case, the volume directly over the F atoms is effectively excluded to the hydration water, thus suggesting strained H-bonds, another indication of their relative weakness.

It seems unsurprising that the discussed 3D spectra are overall very similar to the high-resolution B$\cdots$O and P$\cdots$O spatial distribution functions (SDFs) analyzed recently.[21] This confirms the subtle interplay of structural and dynamical effects in the hydration shells of the studied aqueous anions. Even in the case of BF_4^- and PF_6^-, where the mean anion–water H-bond persistence time is on the order of 0.1–0.2 ps only,[21] the solute–solvent dipolar coupling leaves a persistent mark on the shape of the IR spectrum when examined in a fully 3D picture.

Conclusions

The peculiar nature of the hydrated fluorinated anions (BF_4^- and PF_6^-) has for a long time attracted the attention of the physical chemistry community, with a plethora of experiments confirming their unusually strong effect exerted on the stretching band of water, which their blue-shift to an unparalleled extent. These investigations find here a solid computational

backup from AIMD simulations that accurately reproduce the observed band shift, offering numerous interpretative opportunities due to their ability to not only provide the total IR spectrum, but also to enable its dissection into the spatial-temporal correlations that underlie the IR response of an aqueous solution.

Basing on earlier simple attempts to separate the IR spectrum into solute and solvent contributions, we demonstrate how the progressive inclusion of more and more solvent molecules that are accounted for in the distance-dependent IR spectrum of an aqueous anion unfolds the spectral picture from the "nucleus" of a water-polarized solute to the limit of the spectrum of the entire solution. Between the two extremes, the distance-dependent spectrum uniquely captures the IR response of the solute together with the adjacent water molecules that significantly differ spectrally from the bulk solvent. This is possible because the polarizability of the studied anions is sufficient for them to acquire a sizable induced dipole moment in aqueous solution that in turn allows the solute to efficiently couple its electron density dynamics with the dipolar fluctuations of water molecules in its first hydration sphere. On the other hand, although the polarization of H_2O by the anions is deemed insignificant, the differences in their H-bonding ability to water enforces the shift of its stretching vibration band. These mutual solute–solvent influences are the decisive factor in the shape of the overall IR spectrum of the solution that is here seen to be modulated by intermolecular interactions.

The qualitative nature of the changes observed in the unfolding distance-dependent spectra can be turned quantitative by resorting to the spectral analysis techniques originating from chemometrics. The uniquely defined "crossover" cutoff radius that separates the solute-dominated and bulk solvent-like regimes in the $\alpha^{\mathrm{R}}_{\mathrm{ion}}(\tilde{\nu}, R_c)$ spectra provides the number of spectrally affected solvent molecules and the exact shape of the affected spectrum, thus offering a unique way of comparison of AIMD simulation results with the relevant experimental data. Accordingly, we are able to reproduce both the unparalleled blue shift of the ν_{OH} band of liquid water and the number of affected H_2O molecules for aqueous BF_4^- and PF_6^-.

On top of the distance-dependent spectrum, the detailed nature of the solute–solvent couplings in the IR is best visualized with the aid of the solute-centered radially-resolved cross-correlation spectra. They illustrate clearly the mutual nature of the intermolecular interactions in the solution with ion shifting the stretching vibration of liquid water and water forcing the ion to exhibit IR resonances with no underlying vibrational activity in a concerted manner. Going beyond the radially-resolved approximation, here we examine for the first time the fully spatially-resolved spectra of aqueous solutes, exploiting the fact that the studied anions offer a possibility to define an unambiguous local reference frame due to their rigidity and stability. In the case of BF_4^- and PF_6^-, pronounced correlations of dipolar fluctuations are seen to decisively shape the IR spectrum of water directly affected by the presence of the solute, imprinting a unique 3D pattern on it.

To sum up, theoretical IR spectroscopy based on the analysis of AIMD simulations—that explicitly take into account the crucial many-body polarization effects—is here shown to significantly complement the experimental IR spectroscopy. In particular, its power lies not only in the mere reproduction of the experimental results, but in particular in the opportunity to obtain a molecular level picture of the investigated hydration phenomena without any external input from the experiment. Therefore, such theoretical spectra possess also an appreciable predictive power that might be used in the case of "problematic" solutes that are difficult to approach experimentally.

Acknowledgement

This work was supported by a special habilitation grant from the statutory fund of the Chemical Faculty, Gdańsk University of Technology. Calculations were performed at ICM Warsaw (project no. G53-29). I thank Piotr Bruździak for technical assistance with the chemometric analysis of IR spectra and Janusz Stangret for many friendly discussions.

Supporting Information Available

Convergence of radial distribution functions and vibrational density of states with the system size in the AMOEBA force field simulations; modified Figure 5(a) with a magnified IR intensity scale; additional data on the distance-dependent IR spectrum of Cl^-; correlation plot of $\Delta\tilde{\nu}^\circ_{\mathrm{MD}}$ vs $\Delta\tilde{\nu}^\circ_{\mathrm{exp}}$. This material is available free of charge via the Internet at `http://pubs.acs.org/`.

References

(1) Ball, P. Water as an Active Constituent in Cell Biology. *Chem. Rev.* **2008**, *108*, 74–108.

(2) Ball, P. *Life's Matrix - A Biography of Water*; Farrar, Straus and Giroux: New York, 1999.

(3) Millero, F. J. *Physical Chemistry of Natural Waters*; Wiley-Interscience: New York, 2001.

(4) Marcus, Y. Effect of Ions on the Structure of Water: Structure Making and Breaking. *Chem. Rev.* **2009**, *109*, 1346–1370.

(5) Gurney, R. W. *Ionic Processes in Solution*; McGraw-Hill: New York, 1953.

(6) Mancinelli, R.; Botti, A.; Bruni, F.; Ricci, M. A.; Soper, A. K. Hydration of Sodium, Potassium, and Chloride Ions in Solution and the Concept of Structure Maker/Breaker. *J. Phys. Chem. B* **2007**, *111*, 13570–13577.

(7) Bakker, H. J. Structural Dynamics of Aqueous Salt Solutions. *Chem. Rev.* **2008**, *108*, 1456–1473.

(8) Xu, K. Nonaqueous Liquid Electrolytes for Lithium-Based Rechargeable Batteries. *Chem. Rev.* **2004**, *104*, 4303–4417.

(9) Welton, T. Room-Temperature Ionic Liquids. Solvents for Synthesis and Catalysis. *Chem. Rev.* **1999**, *99*, 2071–2083.

(10) Pieniazek, P. A.; Stangret, J. Hydration of tetraethylammonium tetrafluoroborate derived from FTIR spectroscopy. *Vib. Spectrosc.* **2005**, *39*, 81–87.

(11) Śmiechowski, M.; Gojło, E.; Stangret, J. Ionic Hydration in $LiPF_6$, $NaPF_6$, and KPF_6 Aqueous Solutions Derived from Infrared HDO Spectra. *J. Phys. Chem. B* **2004**, *108*, 15938–15943.

(12) Kristiansson, O.; Lindgren, J.; de Villepin, J. A quantitative infrared spectroscopic method for the study of the hydration of ions in aqueous solutions. *J. Phys. Chem.* **1988**, *92*, 2680–2685.

(13) Paquette, J.; Jolicoeur, C. A near-infrared study of the hydration of various ions and nonelectrolytes. *J. Solution Chem.* **1977**, *6*, 403–428.

(14) Walrafen, G. E. Raman Spectral Studies of the Effects Of Solutes and Pressure on Water Structure. *J. Chem. Phys.* **1971**, *55*, 768–792.

(15) Brink, G.; Falk, M. Infrared spectrum of HDO in aqueous solutions of perchlorates and tetrafluoroborates. *Can. J. Chem.* **1970**, *48*, 3019–3025.

(16) Stangret, J.; Gampe, T. Ionic Hydration Behavior Derived from Infrared Spectra in HDO. *J. Phys. Chem. A* **2002**, *106*, 5393–5402.

(17) Nam, D.; Lee, C.; Park, S. Temperature-Dependent Dynamics of Water in Aqueous $NaPF_6$ Solution. *Phys. Chem. Chem. Phys.* **2014**, *16*, 21747–21754.

(18) Son, H.; Nam, D.; Park, S. Real-Time Probing of Hydrogen-Bond Exchange Dynamics in Aqueous $NaPF_6$ Solutions by Two-Dimensional Infrared Spectroscopy. *J. Phys. Chem. B* **2013**, *117*, 13604–13613.

(19) Moilanen, D. E.; Wong, D.; Rosenfeld, D. E.; Fenn, E. E.; Fayer, M. D. Ion–water hydrogen-bond switching observed with 2D IR vibrational echo chemical exchange spectroscopy. *Proc. Natl. Acad. Sci. U. S. A.* **2009**, *106*, 375–380.

(20) Fayer, M. D.; Moilanen, D. E.; Wong, D.; Rosenfeld, D. E.; Fenn, E. E.; Park, S. Water Dynamics in Salt Solutions Studied with Ultrafast Two-Dimensional Infrared (2D IR) Vibrational Echo Spectroscopy. *Acc. Chem. Res.* **2009**, *42*, 1210–1219.

(21) Śmiechowski, M. Anion–water interactions of weakly hydrated anions: molecular dynamics simulations of aqueous $NaBF_4$ and $NaPF_6$. *Mol. Phys.* **2016**, *114*, 1831–1846.

(22) Marx, D.; Hutter, J. *Ab Initio Molecular Dynamics*; Cambridge University Press: Cambridge, 2009.

(23) Schienbein, P.; Schwaab, G.; Forbert, H.; Havenith, M.; Marx, D. Correlations in the Solute–Solvent Dynamics Reach Beyond the First Hydration Shell of Ions. *J. Phys. Chem. Lett.* **2017**, *8*, 2373–2380.

(24) Śmiechowski, M.; Sun, J.; Forbert, H.; Marx, D. Solvation shell resolved THz spectra of simple aqua ions – distinct distance- and frequency-dependent contributions of solvation shells. *Phys. Chem. Chem. Phys.* **2015**, *17*, 8323–8329.

(25) Śmiechowski, M.; Forbert, H.; Marx, D. Spatial decomposition and assignment of infrared spectra of simple ions in water from mid-infrared to THz frequencies: Li^+(aq) and F^-(aq). *J. Chem. Phys.* **2013**, *139*, 014506.

(26) Śmiechowski, M.; Krakowiak, J.; Bruździak, P.; Stangret, J. Unique Agreement of Experimental and Computational Infrared Spectroscopy: a Case Study of Lithium Bromide Solvation in an Important Electrochemical Solvent. *Phys. Chem. Chem. Phys.* **2017**, *19*, 9270–9280.

(27) Heyden, M.; Sun, J.; Forbert, H.; Mathias, G.; Havenith, M.; Marx, D. Understanding the Origins of Dipolar Couplings and Correlated Motion in the Vibrational Spectrum of Water. *J. Phys. Chem. Lett.* **2012**, *3*, 2135–2140.

(28) Heyden, M.; Sun, J.; Funkner, S.; Mathias, G.; Forbert, H.; Havenith, M.; Marx, D. Dissecting the THz spectrum of liquid water from first principles via correlations in time and space. *Proc. Natl. Acad. Sci. U.S.A.* **2010**, *107*, 12068–12073.

(29) Iftimie, R.; Tuckerman, M. E. Decomposing total IR spectra of aqueous systems into solute and solvent contributions: A computational approach using maximally localized Wannier orbitals. *J. Chem. Phys.* **2005**, *122*, 214508.

(30) Gaigeot, M.-P.; Sprik, M. Ab Initio Molecular Dynamics Computation of the Infrared Spectrum of Aqueous Uracil. *J. Phys. Chem. B* **2003**, *107*, 10344–10358.

(31) Ramírez, R.; López-Ciudad, T.; Kumar, P.; Marx, D. Quantum corrections to classical time-correlation functions: Hydrogen bonding and anharmonic floppy modes. *J. Chem. Phys.* **2004**, *121*, 3973–3983.

(32) Stangret, J.; Gampe, T. Hydration Sphere of Tetrabutylammonium Cation. FTIR Studies of HDO Spectra. *J. Phys. Chem. B* **1999**, *103*, 3778–3783.

(33) Stangret, J. Solute-affected vibrational spectra of water in $Ca(ClO_4)_2$ aqueous solutions. *Spectrosc. Lett.* **1988**, *21*, 369–381.

(34) Malinowski, E. R. *Factor Analysis in Chemistry, 3rd edn*; Wiley: New York, 2002.

(35) Bruździak, P.; Rakowska, P. W.; Stangret, J. Chemometric Method of Spectra Analysis Leading to Isolation of Lysozyme and CtDNA Spectra Affected by Osmolytes. *Appl. Spectrosc.* **2012**, *66*, 1302–1310.

(36) Bruździak, P.; Panuszko, A.; Stangret, J. Chemometric determination of solute-affected solvent vibrational spectra as a superior way of information extraction on solute solvation phenomena. *Vib. Spectrosc.* **2010**, *54*, 65–71.

(37) Ponder, J. W. *Tinker: Software Tools for Molecular Design, 6.3*; Washington University School of Medicine: Saint Louis, MO, 2014.

(38) Ren, P.; Ponder, J. W. Polarizable atomic multipole water model for molecular mechanics simulation. *J. Phys. Chem. B* **2003**, *107*, 5933–5947.

(39) Grossfield, A.; Ren, P.; Ponder, J. Ion solvation thermodynamics from simulation with a polarizable force field. *J. Am. Chem. Soc.* **2003**, *125*, 15671–15682.

(40) VandeVondele, J.; Krack, M.; Mohamed, F.; Parrinello, M.; Chassaing, T.; Hutter, J. Quickstep: Fast and accurate density functional calculations using a mixed Gaussian and plane waves approach. *Comp. Phys. Commun.* **2005**, *167*, 103–128.

(41) The cp2k Developers Group, cp2k v. 2.3. 2001–2012; `http://www.cp2k.org/`.

(42) Hutter, J.; Iannuzzi, M.; Schiffmann, F.; VandeVondele, J. cp2k: atomistic simulations of condensed matter systems. *WIREs Comput. Mol. Sci.* **2014**, *4*, 15–25.

(43) Becke, A. D. Density-functional exchange-energy approximation with correct asymptotic behavior. *Phys. Rev. A* **1988**, *38*, 3098–3100.

(44) Lee, C.; Yang, W.; Parr, R. G. Development of the Colle-Salvetti correlation-energy formula into a functional of the electron density. *Phys. Rev. B* **1988**, *37*, 785–789.

(45) Grimme, S.; Antony, J.; Ehrlich, S.; Krieg, H. A consistent and accurate *ab initio* parametrization of density functional dispersion correction (DFT-D) for the 94 elements H-Pu. *J. Chem. Phys.* **2010**, *132*, 154104.

(46) Lippert, G.; Hutter, J.; Parrinello, M. A hybrid Gaussian and plane wave density functional scheme. *Mol. Phys.* **1997**, *92*, 477–487.

(47) Goedecker, S.; Teter, M.; Hutter, J. Separable dual-space Gaussian pseudopotentials. *Phys. Rev. B* **1996**, *54*, 1703–1710.

(48) Jonchiere, R.; Seitsonen, A. P.; Ferlat, G.; Saitta, A. M.; Vuilleumier, R. Van der Waals effects in *ab initio* water at ambient and supercritical conditions. *J. Chem. Phys.* **2011**, *135*, 154503.

(49) Marzari, N.; Vanderbilt, D. Maximally localized generalized Wannier functions for composite energy bands. *Phys. Rev. B* **1997**, *56*, 12847–12865.

(50) Iftimie, R.; Thomas, J. W.; Tuckerman, M. E. On-the-fly localization of electronic orbitals in Car–Parrinello molecular dynamics. *J. Chem. Phys.* **2004**, *120*, 2169–2181.

(51) Hale, G. M.; Querry, M. R. Optical constants of water in the 200-nm to 200-μm wavelength region. *Appl. Opt.* **1973**, *12*, 555–563.

(52) Śmiechowski, M. Molecular hydrogen solvated in water – A computational study. *J. Chem. Phys.* **2015**, *143*, 244505.

(53) Marcus, Y. The Standard Partial Molar Volumes of Ions in Solution. Part 4. Ionic Volumes in Water at 0–100 °C. *J. Phys. Chem. B* **2009**, *113*, 10285–10291.

(54) Marcus, Y. The Molar Volumes of Ions in Solution, Part 7. Electrostriction and Hydration Numbers of Aqueous Polyatomic Anions at 25 °C. *J. Phys. Chem. B* **2014**, *118*, 2172–2175.

(55) Yamaguchi, T.; Ohzono, H.; Yamagami, M.; Yamanaka, K.; Yoshida, K.; Wakita, H. Ion hydration in aqueous solutions of lithium chloride, nickel chloride, and caesium chloride in ambient to supercritical water. *J. Mol. Liquids* **2010**, *153*, 2–8.

(56) Mile, V.; Pusztai, L.; Dominguez, H.; Pizio, O. Understanding the Structure of Aqueous Cesium Chloride Solutions by Combining Diffraction Experiments, Molecular Dy-

namics Simulations, and Reverse Monte Carlo Modeling. *J. Phys. Chem. B* **2009**, *113*, 10760–10769.

(57) Bouazizi, S.; Nasr, S. Local order in aqueous lithium chloride solutions as studied by X-ray scattering and molecular dynamics simulations. *J. Mol. Struct.* **2007**, *837*, 206–213.

(58) Bouazizi, S.; Nasr, S.; Jaîdane, N.; Bellissent-Funel, M.-C. Local Order in Aqueous NaCl Solutions and Pure Water: X-ray Scattering and Molecular Dynamics Simulations Study. *J. Phys. Chem. B* **2006**, *110*, 23515–23523.

(59) Dang, L. X.; Schenter, G. K.; Glezakou, V.-A.; Fulton, J. L. Molecular Simulation Analysis and X-ray Absorption Measurement of Ca^{2+}, K^{+} and Cl^{-} Ions in Solution. *J. Phys. Chem. B* **2006**, *110*, 23644–23654.

(60) Mason, P. E.; Ansell, S.; Neilson, G. W. Neutron diffraction studies of electrolytes in null water: a direct determination of the first hydration zone of ions. *J. Phys.: Condens. Matter* **2006**, *18*, 8437–8447.

(61) Soper, A. K.; Weckström, K. Ion solvation and water structure in potassium halide aqueous solutions. *Biophys. Chem.* **2006**, *124*, 180–191.

(62) Nygård, K.; Hakala, M.; Manninen, S.; Hämäläinen, K.; Itou, M.; Andrejczuk, A.; Sakurai, Y. Ion hydration studied by x-ray Compton scattering. *Phys. Rev. B* **2006**, *73*, 024208.

(63) Yamaguchi, T.; Yamagami, M.; Ohzono, H.; Wakita, H.; Yamanaka, K. Chloride-ion hydration in supercritical water by neutron diffraction. *Chem. Phys. Lett.* **1996**, *252*, 317–321.

(64) Powell, D. H.; Neilson, G. W.; Enderby, J. E. The structure of Cl^{-} in aqueous solution:

an experimental determination of $g_{\mathrm{ClH}}(r)$ and $g_{\mathrm{ClO}}(r)$. *J. Phys.: Condens. Matter* **1993**, *5*, 5723–5730.

(65) Yamanaka, K.; Yamagami, M.; Takamuku, T.; Yamaguchi, T.; Wakita, H. X-ray Diffraction Study on Aqueous Lithium Chloride Solution in the Temperature Range 138–373 K. *J. Phys. Chem.* **1993**, *97*, 10835–10839.

(66) Ohtaki, H.; Fukushima, N. A Structural Study of Saturated Aqueous Solutions of Some Alkali Halides by X-Ray Diffraction. *J. Solution Chem.* **1992**, *21*, 23–38.

(67) Gaiduk, A. P.; Galli, G. Local and Global Effects of Dissolved Sodium Chloride on the Structure of Water. *J. Phys. Chem. Lett.* **2017**, *8*, 1496–1502.

(68) Pham, T. A.; Ogitsu, T.; Lau, E. Y.; Schwegler, E. Structure and dynamics of aqueous solutions from PBE-based first-principles molecular dynamics simulations. *J. Chem. Phys.* **2016**, *145*, 154501.

(69) Bankura, A.; Santra, B.; DiStasio, R. A.; Swartz, C. W.; Klein, M. L.; Wu, X. A systematic study of chloride ion solvation in water using van der Waals inclusive hybrid density functional theory. *Mol. Phys.* **2015**, *113*, 2842–2854.

(70) Gaiduk, A. P.; Zhang, C.; Gygi, F.; Galli, G. Structural and electronic properties of aqueous NaCl solutions from ab initio molecular dynamics simulations with hybrid density functionals. *Chem. Phys. Lett.* **2014**, *604*, 89–96.

(71) Ding, Y.; Hassanali, A. A.; Parrinello, M. Anomalous water diffusion in salt solutions. *Proc. Natl. Acad. Sci. U. S. A.* **2014**, *111*, 3310–3315.

(72) Bankura, A.; Carnevale, V.; Klein, M. L. Hydration structure of salt solutions from ab initio molecular dynamics. *J. Chem. Phys.* **2013**, *138*, 014501.

(73) Ge, L.; Bernasconi, L.; Hunt, P. Linking electronic and molecular structure: insight into aqueous chloride solvation. *Phys. Chem. Chem. Phys.* **2013**, *15*, 13169–13183.

(74) Galamba, N.; Mata, R. A.; Cabral, B. J. C. Electronic Excitation of Cl^- in Liquid Water and at the Surface of a Cluster: A Sequential Born–Oppenheimer Molecular Dynamics/Quantum Mechanics Approach. *J. Phys. Chem. A* **2009**, *113*, 14684–14690.

(75) Guàrdia, E.; Skarmoutsos, I.; Masia, M. On Ion and Molecular Polarization of Halides in Water. *J. Chem. Theory Comput.* **2009**, *5*, 1449–1453.

(76) Scipioni, R.; Schmidt, D. A.; Boero, M. A first principles investigation of water dipole moment in a defective continuous hydrogen bond network. *J. Chem. Phys.* **2009**, *130*, 024502.

(77) Schmidt, D. A.; Scipioni, R.; Boero, M. Water Solvation Properties: An Experimental and Theoretical Investigation of Salt Solutions at Finite Dilution. *J. Phys. Chem. A* **2009**, *113*, 7725–7729.

(78) Mallik, B. S.; Semparithi, A.; Chandra, A. A first principles theoretical study of vibrational spectral diffusion and hydrogen bond dynamics in aqueous ionic solutions: D_2O in hydration shells of Cl^- ions. *J. Chem. Phys.* **2008**, *129*, 194512.

(79) Petit, L.; Vuilleumier, R.; Maldivi, P.; Adamo, C. Ab Initio Molecular Dynamics Study of a Highly Concentrated LiCl Aqueous Solution. *J. Chem. Theory Comput.* **2008**, *4*, 1040–1048.

(80) Heuft, J. M.; Meijer, E. J. Density functional theory based molecular-dynamics study of aqueous chloride solvation. *J. Chem. Phys.* **2003**, *119*, 11788–11791.

(81) Takeuchi, M.; Matubayasi, N.; Kameda, Y.; Minofar, B.; Ishiguro, S.-I.; Umebayashi, Y. Free-Energy and Structural Analysis of Ion Solvation and Contact Ion-Pair Formation of Li^+ with BF_4^- and PF_6^- in Water and Carbonate Solvents. *J. Phys. Chem. B* **2012**, *116*, 6476–6487.

(82) Raugei, S.; Klein, M. L. An ab initio study of water molecules in the bromide ion solvation shell. *J. Chem. Phys.* **2009**, *116*, 196–202.

(83) DiStasio, R. A.; Santra, B.; Li, Z.; Wu, X.; Car, R. The individual and collective effects of exact exchange and dispersion interactions on the ab initio structure of liquid water. *J. Chem. Phys.* **2014**, *141*, 084502.

(84) McGrath, M. J.; Siepmann, J. I.; Kuo, I.-F. W.; Mundy, C. J. Spatial correlation of dipole fluctuations in liquid water. *Mol. Phys.* **2007**, *105*, 1411–1417.

(85) Sharma, M.; Resta, R.; Car, R. Dipolar Correlations and the Dielectric Permittivity of Water. *Phys. Rev. Lett.* **2007**, *98*, 247401.

(86) Silvestrelli, P. L.; Parrinello, M. Water molecule dipole in the gas and in the liquid phase. *Phys. Rev. Lett.* **1999**, *82*, 3308–3311.

(87) Silvestrelli, P. L.; Parrinello, M. Structural, electronic, and bonding properties of liquid water from first principles. *J. Chem. Phys.* **1999**, *111*, 3572–3580.

(88) Bertie, J. E.; Lan, Z. Infrared Intensities of Liquids XX: The Intensity of the OH Stretching Band of Liquid Water Revisited, and the Best Current Values of the Optical Constants of H_2O(l) at 25°C between 15,000 and 1 cm^{-1}. *Appl. Spectrosc.* **1996**, *50*, 1047–1057.

(89) Zhang, C.; Wu, J.; Galli, G.; Gygi, F. Structural and Vibrational Properties of Liquid Water from van der Waals Density Functionals. *J. Chem. Theory Comput.* **2011**, *7*, 3054–3061.

(90) Lee, H.-S.; Tuckerman, M. E. Dynamical properties of liquid water from *ab initio* molecular dynamics performed in the complete basis set limit. *J. Chem. Phys.* **2007**, *126*, 164501.

(91) Marsalek, O.; Markland, T. E. Quantum Dynamics and Spectroscopy of Ab Initio Liquid Water: The Interplay of Nuclear and Electronic Quantum Effects. *J. Phys. Chem. Lett.* **2017**, *8*, 1545–1551.

(92) Bergström, P.; Lindgren, J.; Kristiansson, O. H/D Isotope Effects in Aqueous Solutions of $Ni(ClO_4)_2$, $Ni(CF_3)_2$ and $Mg(ClO_4)_2$ as studied by Infrared Spectroscopy. *J. Mol. Liquids* **1991**, *50*, 197–206.

(93) Lindgren, J.; Hermansson, K.; Wojcik, M. J. Theoretical Simulation and Experimental Determination of OH and OD Stretching Bands of Isotopically Diluted HDO Molecules in Aqueous Electrolyte Solutions. *J. Phys. Chem.* **1993**, *97*, 5254–5259.

(94) Wojcik, M. J.; Hermansson, K.; Lindgren, J.; Ojamäe, L. Theoretical simulation of OH and OD stretching bands of isotopically diluted HDO molecules in aqueous solution. *Chem. Phys.* **1993**, *171*, 189–201.

(95) Śmiechowski, M.; Stangret, J. ATR FT-IR H_2O spectra of acidic aqueous solutions. Insights about proton hydration. *J. Mol. Struct.* **2008**, *878*, 104–115.

(96) Śmiechowski, M.; Stangret, J. Proton hydration in aqueous solution: Fourier transform infrared studies of HDO spectra. *J. Chem. Phys.* **2006**, *125*, 204508.

(97) Kleeberg, H.; Luck, W. A. P. Experimental Tests of the H-Bond Cooperativity. *Z. Phys. Chem.* **1989**, *270*, 613–625.

(98) Zhang, C.; Hutter, J.; Sprik, M. Computing the Kirkwood g-Factor by Combining Constant Maxwell Electric Field and Electric Displacement Simulations: Application to the Dielectric Constant of Liquid Water. *J. Phys. Chem. Lett.* **2016**, *7*, 2696–2701.

(99) Śmiechowski, M.; ; Stangret, J. Vibrational spectroscopy of semiheavy water (HDO) as a probe of solute hydration. *Pure Appl. Chem.* **2010**, *82*, 1869–1887.

(100) Baul, U.; Kanth, J. M. P.; Anishetty, R.; Vemparala, S. Effect of simple solutes on the long range dipolar correlations in liquid water. *J. Chem. Phys.* **2016**, *144*, 104502.

(101) Śmiechowski, M. Visualizing spatially decomposed intermolecular correlations in the infrared spectra of aprotic liquids. *J. Mol. Graph.* **2017**, *78*, 148–157.

Graphical TOC Entry

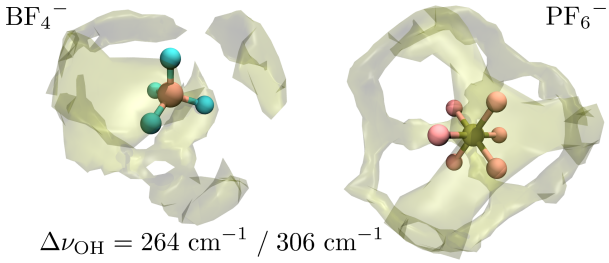

$\Delta\nu_{\mathrm{OH}} = 264\ \mathrm{cm}^{-1}\ /\ 306\ \mathrm{cm}^{-1}$

$$\alpha_{\times}(\tilde{\nu}, \boldsymbol{r}) \propto \int_{-\infty}^{\infty} dt\, e^{-i\omega t}\, C_{\mu\rho}(t, \boldsymbol{r})$$

Supporting information for:

Unusual Influence of the Fluorinated Anions on the Stretching Vibrations of Liquid Water

Maciej Śmiechowski*

Department of Physical Chemistry, Chemical Faculty, Gdańsk University of Technology, Narutowicza 11/12, 80-233 Gdańsk, Poland

E-mail: Maciej.Smiechowski@pg.edu.pl

Convergence of Results with System Size

Since the 64 H_2O molecules used to solvate the studied ions allow for inclusion of the entire first hydration sphere and the strained second hydration sphere only, the question whether the applied system size is sufficient for the present purpose is a pertinent one. Therefore, the convergence of representative static and dynamic observables was thoroughly checked using the classical force field simulations with the TINKER-HP code.[1]

Each ion (Cl^-, BF_4^-, or PF_6^-) was solvated with the progressively increasing number of water molecules (up to 512 H_2O) and the interactions were represented using the AMOEBA force field.[2,3] Each system was contained in a cubic cell with applied periodic boundary conditions and prepared at the volume corresponding to the partial molar volumes of the anions as reported in Table 1 in the main text combined with the molar volume of pure AMOEBA water (18.06 $cm^3\ mol^{-1}$).[4] The resulting cell sizes are reported in Table S1. After

Table S1: Box Lengths for the Systems with Varying Number of Water Molecules

Ion	L_{64} (Å)	L_{128} (Å)	L_{256} (Å)	L_{512} (Å)
Cl^-	12.516	15.714	19.763	24.877
BF_4^-	12.585	15.758	19.791	24.895
PF_6^-	12.655	15.803	19.819	24.913

initial equilibration for 1 ns at $T = 298$ K in the canonical (NVT) ensemble—with the constant temperature conditions maintained by weakly coupling to an external bath[5] with a time constant of 0.1 ps—the NVT trajectory was continued and 32 initial conditions were sampled from it every 10 ps in order to spawn production run microcanonical (NVE) trajectories of 20 ps length each. All the reported observables were averaged over the 32 NVE runs thus obtaining proper canonical averages.[6]

The time step was set to 0.5 fs and the production trajectories were saved every 2 fs. The equations of motion were integrated with a modified Beeman algorithm.[7] The electrostatic interactions were calculated with the smooth particle mesh Ewald (SPME) method,[8] and the van der Waals interactions were represented by a buffered 14–7 potential as defined in

AMOEBA.[2,9] In both cases the real space cutoff was set to half the simulation box length, while the grid spacing for SPME was ~ 0.5 Å. The convergence criterion for the induced dipoles in the self-consistent iterative procedure was set to 10^{-4} D.

Radial Distribution Functions

The static structure of the hydration shells of the investigated anions is visualized with the help of radial distribution functions (RDFs) in Figure 1 in the main text. Since the characteristic parameters of the RDFs, as well as their agreement with previous computational and experimental studies are discussed in detail in the main text, we focus here on the convergence of the RDFs with the increasing system size. The A$\cdots$O and A$\cdots$H RDFs for the larger systems in comparison to the 64 H_2O systems used in AIMD simulations are shown in Figures S1, S2, and S3 for A = Cl^-, A = BF_4^-, and A = PF_6^-, respectively.

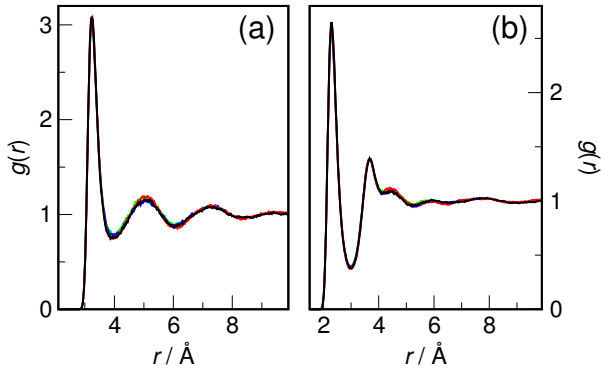

Figure S1: Radial distribution functions, $g(r)$, for (a) Cl$\cdots$O and (b) Cl$\cdots$H pairs in the studied $Cl^-(H_2O)_n$ systems for $n = 64$ (green), 128 (blue), 256 (red), and 512 (black).

It is immediately seen that for Cl^- both $g_{ClO}(r)$ (Figure S1(a)) and $g_{ClH}(r)$ (Figure S1(b)) are essentially independent of the system size, which is not surprising considering that even the smallest $Cl^-(H_2O)_{64}$ system is sufficient to contain two entire hydration spheres, since the second minimum in $g_{ClO}(r)$ is found at ~ 6 Å. On the other hand, while for BF_4^- and PF_6^- $g_{BO}(r)$ and $g_{PO}(r)$ RDFs display exactly the same features, see Figures S2(a) and S3(a), minor variations in the relative proportions of different features are particularly apparent

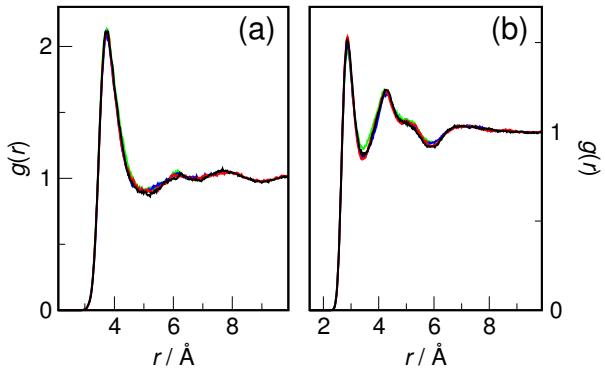

Figure S2: Radial distribution functions, $g(r)$, for (a) B$\cdots$O and (b) B$\cdots$H pairs in the studied $BF_4^-(H_2O)_n$ systems for $n = 64$ (green), 128 (blue), 256 (red), and 512 (black).

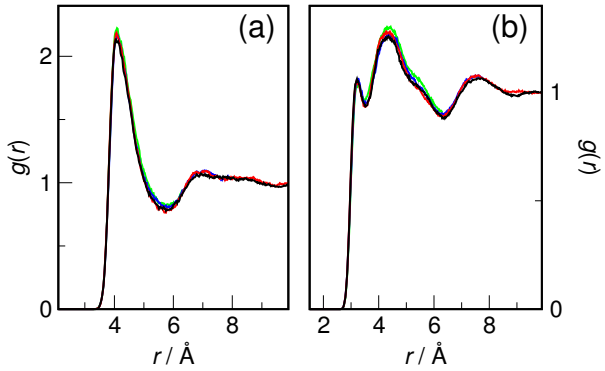

Figure S3: Radial distribution functions, $g(r)$, for (a) P$\cdots$O and (b) P$\cdots$H pairs in the studied $PF_6^-(H_2O)_n$ systems for $n = 64$ (green), 128 (blue), 256 (red), and 512 (black).

in Figures S2(b) and S3(b) for $g_{BH}(r)$ and $g_{PH}(r)$, respectively. In order to estimate the influence of these variations on the state of the hydration spheres of the fluorinated anions, we present in Tables S2 and S3 a more detailed description of the discussed RDFs, including locations of the maxima and minima and the integration results.

It is apparent that the intermolecular distances at maxima and minima are remarkably preserved when increasing the system size (note that the size of the RDF bin, and thus the resolution of the curves, is 0.02 Å). The number of oxygen and hydrogen atoms up to the first or second minimum indeed tends to grow with n, however, the variation is minor and the results for the smallest system are already very close to the previously reported ones from more extensive simulations, $N_{BO}^{(1)} = 17.6$ and $N_{PO}^{(1)} = 23.4$.[10]

Table S2: Radial Distribution Functions Parameters for the Studied $BF_4^-(H_2O)_n$ Systems: the Location of the First Maximum and First Minimum of $g_{BO}(r)$ and the Location of the First and the Second Maximum and Minimum of $g_{BH}(r)$, Including Respective Integrations

n	$R_{BO}^{(1)}$ (Å)	$r_{BO}^{(1)}$ (Å)	$N_{BO}^{(1)}$	$R_{BH}^{(1)}$ (Å)	$r_{BH}^{(1)}$ (Å)	$N_{BH}^{(1)}$	$R_{BH}^{(2)}$ (Å)	$r_{BH}^{(2)}$ (Å)	$N_{BH}^{(2)}$
64	3.75	5.17	17.4	2.85	3.45	7.3	4.19	5.85	52.7
128	3.71	5.19	17.3	2.87	3.45	7.4	4.23	5.85	52.6
256	3.73	5.19	17.6	2.87	3.41	7.1	4.23	5.85	53.5
512	3.73	5.21	17.8	2.85	3.41	7.2	4.23	5.87	54.1

Table S3: Radial Distribution Functions Parameters for the Studied $PF_6^-(H_2O)_n$ Systems: the Location of the First Maximum and First Minimum of $g_{PO}(r)$ and the Location of the First and the Second Maximum and Minimum of $g_{PH}(r)$, Including Respective Integrations

n	$R_{PO}^{(1)}$ (Å)	$r_{PO}^{(1)}$ (Å)	$N_{PO}^{(1)}$	$R_{PH}^{(1)}$ (Å)	$r_{PH}^{(1)}$ (Å)	$N_{PH}^{(1)}$	$R_{PH}^{(2)}$ (Å)	$r_{PH}^{(2)}$ (Å)	$N_{PH}^{(2)}$
64	4.09	5.73	23.6	3.25	3.51	4.6	4.39	6.31	64.5
128	4.09	5.79	24.2	3.25	3.49	4.6	4.35	6.33	65.4
256	4.07	5.75	23.9	3.23	3.49	4.7	4.35	6.31	65.3
512	4.05	5.75	23.9	3.23	3.49	4.7	4.35	6.33	66.2

Concluding, while the smallest system shows a very slight tendency for "incomplete" hydration (i.e., lower number of oxygen or hydrogen atoms counted up to the consecutive minima in RDFs), the extent of this effect is insignificant.

Vibrational Density of States

While the intricacies of the spatially-resolved IR spectra cannot be reasonably expected to be captured in the force field simulations, the vibrational dynamics of the system may be represented by vibrational density of states (VDOS), which is sensitive to the atomic motion rather than dipolar correlations. It was previously demonstrated that VDOS is fairly well preserved between popular water models and AIMD simulations.[11]

The VDOS intensities of the entire system, ion, and water for the larger systems in comparison to the 64 H_2O systems used in AIMD simulations are shown in Figures S4, S5, and S6 for Cl^-, BF_4^-, and PF_6^-, respectively. Unlike for Cl^- (see Figure S4(a)),

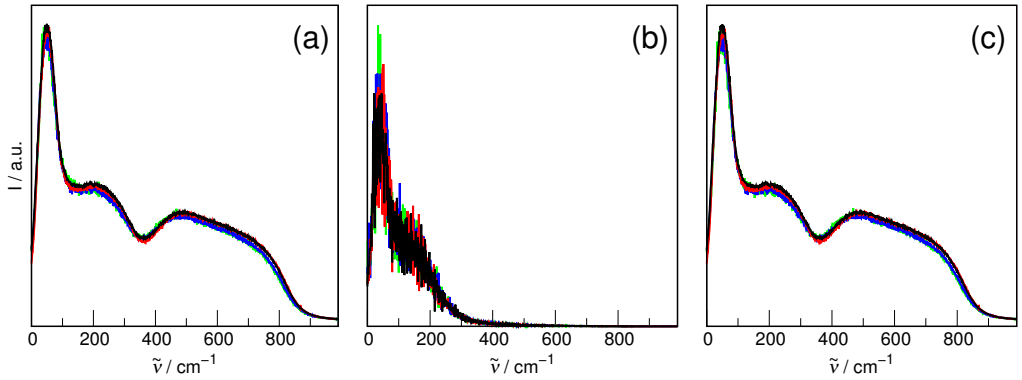

Figure S4: Vibrational density of states for (a) entire system, (b) anion, and (c) water in the studied $Cl^-(H_2O)_n$ systems for $n = 64$ (green), 128 (blue), 256 (red), and 512 (black).

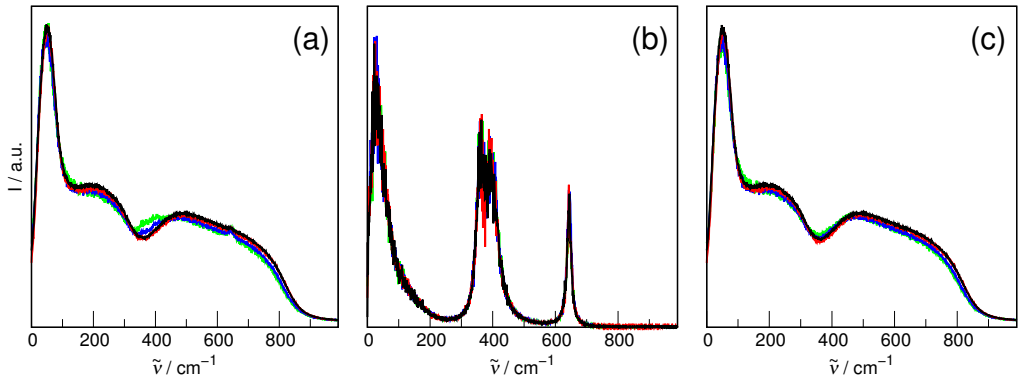

Figure S5: Vibrational density of states for (a) entire system, (b) anion, and (c) water in the studied $BF_4^-(H_2O)_n$ systems for $n = 64$ (green), 128 (blue), 256 (red), and 512 (black).

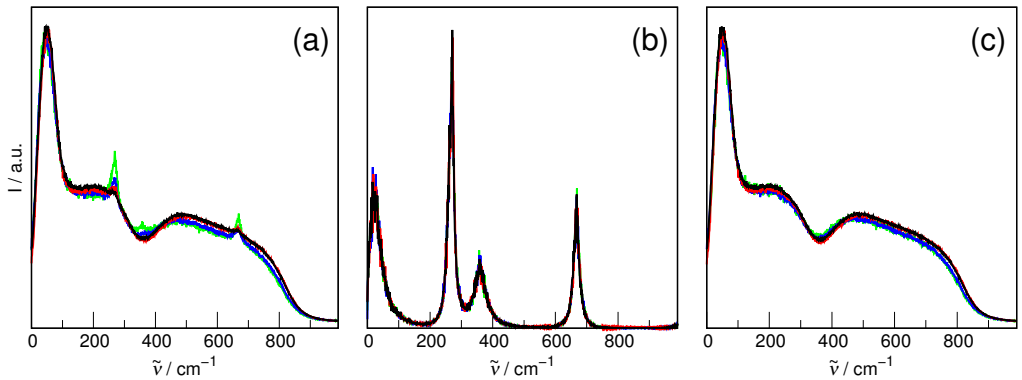

Figure S6: Vibrational density of states for (a) entire system, (b) anion, and (c) water in the studied $PF_6^-(H_2O)_n$ systems for $n = 64$ (green), 128 (blue), 256 (red), and 512 (black).

for BF_4^- and PF_6^- a slight variation of the VDOS intensity is noticeable in Figures S5(a) and S6(a), respectively. The smaller systems evidently display weak additional bands in the far–IR region. However, the comparison with the corresponding anion VDOS intensity (see Figure S4(b), S5(b), and S6(b) for Cl^-, BF_4^-, and PF_6^-, respectively) reveals that these bands are just due to the intramolecular motion of the anions in the two latter cases. They are more prominent in the case of smaller systems simply due to the higher relative concentration of the anion.

Additionally, it is clear that the VDOS intensity of water (see Figure S4(c), S5(c), and S6(c) for Cl^-, BF_4^-, and PF_6^-, respectively) is almost constant with increasing system size, which in turn proves that the molecular motion of water is not hindered by the possible unfavorable intra-shell intermolecular interactions in the second hydration shell. Concluding, the vibrational dynamics of the molecules seems to be independent of the system size and thus strongly supports the premise that also IR response (which is a result of *both* vibrational dynamics *and* dynamic polarization effects) may be reasonably expected to be captured properly even in the smallest systems as used in the AIMD simulations.

Radially-resolved Spectrum of Cl^-

In the main text, a reference to the radially-resolved spectrum of Cl^- with a modified color palette is given. The original palette range is chosen to faithfully represent the entire IR spectrum modulation for all the studied anions in the permissible radius range. In order to amplify the effects visible for Cl^- beyond the first hydration shell, we show here a modified version of Figure 5(a) with an artificially imposed intensity cutoff, see Figure S7.

Distance-dependent Spectrum of Cl^-

In the main text, a reference to the details of the modulation of $\alpha^{\mathrm{R}}_{\mathrm{ion}}(\tilde{\nu}, R_c)$ spectra for Cl^- is given. Unlike in Figure 4(a), where the selected distance-dependent spectrum for Cl^-

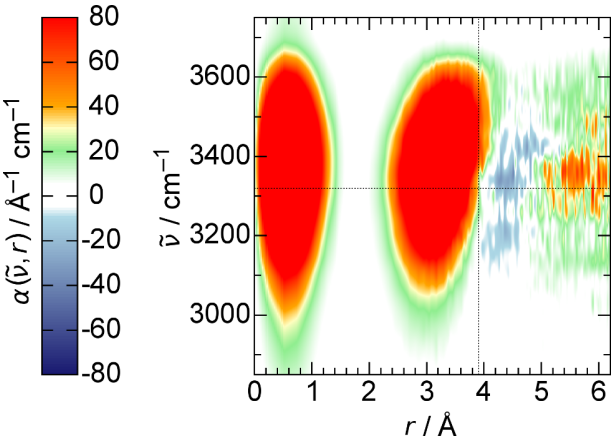

Figure S7: Radially-resolved IR spectrum in the water OH stretching vibrations range for Cl^- with a magnified color palette range. Thin horizontal line indicates the band position at maximum for bulk water, while thin vertical line shows the extent of the first hydration shell as inferred from the first minimum in $g_{ClO}(r)$.

at $R_c^\circ = 3.8$ Å looks notably similar to the bulk water spectrum, particularly in contrast with the fluorinated anions, Figure S8(a) illustrates the intensity modulation sampled at the maximum of the bulk water band, while Figure S8(a) provides a direct comparison with the bulk spectrum.

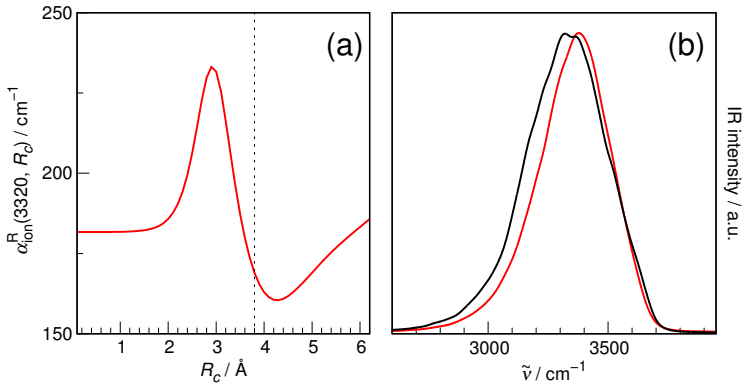

Figure S8: (a) The intensity modulation of the $\alpha^{\mathrm{R}}_{\mathrm{ion}}(\tilde{\nu}, R_c)$ spectra for Cl^- at $\tilde{\nu} = 3320$ cm^{-1} (the bulk water band position) with increasing R_c. Thin vertical line corresponds to the $R_c^\circ = 3.8$ Å value selected with the spectral similarity method. (b) The distance-dependent IR spectrum, $\alpha^{\mathrm{R}}_{\mathrm{ion}}(\tilde{\nu}, R_c)$, in the water OH stretching vibrations range at $R_c^\circ = 3.8$ Å for Cl^- (red) compared with the bulk water IR spectrum (black). Both spectra are scaled to the same intensity at maximum.

Correlation Plot of $\Delta\tilde{\nu}^{\circ}_{\mathbf{MD}}$ vs $\Delta\tilde{\nu}^{\circ}_{\mathbf{exp}}$

In the main text, the exceptionally linear correlation between the shift of the OH stretching band with respect to the bulk H_2O position at maximum for the solutes studied here with AIMD and the experimental shift of the OD stretching band of HDO[12] is mentioned, basing on the data from Table 2 in the main text. This correlation plot is shown in Figure S9.

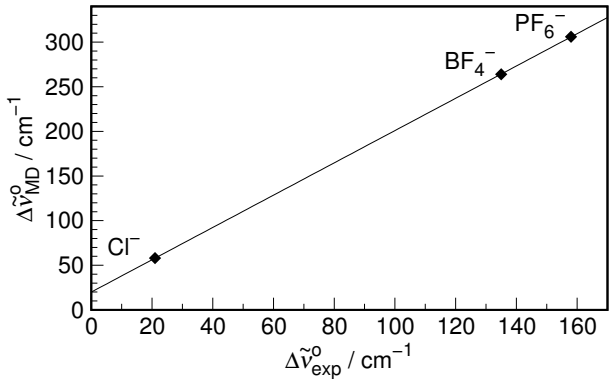

Figure S9: The dependence of $\Delta\tilde{\nu}^{\circ}_{\mathrm{MD}}$ on $\Delta\tilde{\nu}^{\circ}_{\mathrm{exp}}$. Solid line shows the linear least-squares fit ($\Delta\tilde{\nu}^{\circ}_{\mathrm{MD}} = 1.81\,\Delta\tilde{\nu}^{\circ}_{\mathrm{exp}} + 20.0, R^2 \approx 1$). Experimental data taken from ref 12.

While the quality of the linear relationship is exceptional, the extent of this effect demands an additional explanation. The present slope (1.81) is appreciably higher than the experimental value based on limited data concerning identical solutes dissolved in HDO/H_2O or HDO/D_2O (1.44).[13] We tentatively ascribe this effect to the lack of nuclear quantum effects (NQE) in our AIMD simulations. It is well-known that the inclusion of NQE increases the proton-sharing tendency of H-bonds in liquid water, thus lowering the vibrational frequency.[14] On the other hand, the latter is also linearly related to the strength of the local electric field component taken in the direction of the vibrating oscillator, a property that is also strongly influenced by NQE.[15] While all these effects are crucial for the "water ions" (i.e., $H^+(aq)$ and $OH^-(aq)$),[16] a growing computational evidence suggests that "perturbations" of the H-bond network of water (such as solvated ions) modulate the stability of the quantum fluctuations that are already present in bulk liquid water rather than introduce entirely new effects.[17] The general "softening" effect of NQE on the ion–water interactions

is also well documented for the enthalpies of formation of aqueous clusters of iodide.[18] Thus, we are fairly confident that NQE are the principal underlying cause of the overestimation of the frequency shifts from the bulk water position induced by aqueous ions in the present AIMD simulations.

References

(1) Lagardere, L.; Jolly, L.-H.; Lipparini, F.; Aviat, F.; Stamm, B.; Jing, Z. F.; Harger, M.; Torabifard, H.; Cisneros, G. A.; Schnieders, M. J.; Gresh, N.; Maday, Y.; Ren, P. Y.; Ponder, J. W.; Piquemal, J.-P. Tinker-HP: a massively parallel molecular dynamics package for multiscale simulations of large complex systems with advanced point dipole polarizable force fields. *Chem. Sci.* **2018**, *9*, 956–972.

(2) Ren, P.; Ponder, J. W. Polarizable atomic multipole water model for molecular mechanics simulation. *J. Phys. Chem. B* **2003**, *107*, 5933–5947.

(3) Grossfield, A.; Ren, P.; Ponder, J. Ion solvation thermodynamics from simulation with a polarizable force field. *J. Am. Chem. Soc.* **2003**, *125*, 15671–15682.

(4) Śmiechowski, M. Molecular hydrogen solvated in water – A computational study. *J. Chem. Phys.* **2015**, *143*, 244505.

(5) Berendsen, H. J. C.; Postma, J. P. M.; van Gunsteren, W. F.; DiNola, A.; Haak, J. R. Molecular Dynamics with Coupling to an External Bath. *J. Chem. Phys.* **1984**, *81*, 3684–3690.

(6) Tuckerman, M. *Statistical Mechanics: Theory and Molecular Simulation*; Oxford University Press: New York, 2010.

(7) Beeman, D. Some Multistep Methods for use in Molecular Dynamics Calculations. *J. Comp. Phys.* **1976**, *20*, 130–139.

(8) Essmann, U.; Perera, L.; Berkowitz, M. L.; Darden, T.; Lee, H.; Pedersen, L. G. A smooth particle mesh Ewald method. *J. Chem. Phys.* **1995**, *103*, 8577–8593.

(9) Ren, P.; Ponder, J. W. Consistent treatment of inter- and intramolecular polarization in molecular mechanics calculations. *J. Comput. Chem.* **2002**, *23*, 1497–1506.

(10) Śmiechowski, M. Anion–water interactions of weakly hydrated anions: molecular dynamics simulations of aqueous $NaBF_4$ and $NaPF_6$. *Mol. Phys.* **2016**, *114*, 1831–1846.

(11) Heyden, M.; Sun, J.; Forbert, H.; Mathias, G.; Havenith, M.; Marx, D. Understanding the Origins of Dipolar Couplings and Correlated Motion in the Vibrational Spectrum of Water. *J. Phys. Chem. Lett.* **2012**, *3*, 2135–2140.

(12) Stangret, J.; Gampe, T. Ionic Hydration Behavior Derived from Infrared Spectra in HDO. *J. Phys. Chem. A* **2002**, *106*, 5393–5402.

(13) Bergström, P.; Lindgren, J.; Kristiansson, O. H/D Isotope Effects in Aqueous Solutions of $Ni(ClO_4)_2$, $Ni(CF_3)_2$ and $Mg(ClO_4)_2$ as studied by Infrared Spectroscopy. *J. Mol. Liquids* **1991**, *50*, 197–206.

(14) Marsalek, O.; Markland, T. E. Quantum Dynamics and Spectroscopy of Ab Initio Liquid Water: The Interplay of Nuclear and Electronic Quantum Effects. *J. Phys. Chem. Lett.* **2017**, *8*, 1545–1551.

(15) Paesani, F.; Xantheas, S. S.; Voth, G. A. Infrared Spectroscopy and Hydrogen-Bond Dynamics of Liquid Water from Centroid Molecular Dynamics with an Ab Initio-Based Force Field. *J. Phys. Chem. B* **2009**, *113*, 13118–13130.

(16) Agmon, N.; Bakker, H. J.; Campen, R. K.; Henchman, R. H.; Pohl, P.; Roke, S.; Thämer, M.; Hassanali, A. Protons and Hydroxide Ions in Aqueous Systems. *Chem. Rev.* **2016**, *116*, 7642–7672.

(17) Ceriotti, M.; Cuny, J.; Parrinello, M.; Manolopoulos, D. E. Nuclear quantum effects and hydrogen bond fluctuations in water. *Proc. Natl. Acad. Sci. U. S. A.* **2013**, *110*, 15591–15596.

(18) Gai, H.; Schenter, G. K.; Dang, L. X.; Garrett, B. C. Quantum statistical mechanical simulation of the ion–water cluster $I^-(H_2O)_n$: The importance of nuclear quantum effects and anharmonicity. *J. Chem. Phys.* **1996**, *105*, 8835–8841.